
Article:
Kirkham, JD, Hogan, KA, Larter, RD et al. (9 more authors) (2022) Tunnel valley formation beneath deglaciating mid-latitude ice sheets: observations and modelling. Quaternary Science Reviews. 107680. ISSN 0277-3791

https://doi.org/10.1016/j.quascirev.2022.107680

Quaternary Science Reviews xxx (xxxx) xxx

Contents lists available at ScienceDirect

Quaternary Science Reviews

journal homepage: www.elsevier.com/locate/quascirev

Tunnel valley formation beneath deglaciating mid-latitude ice sheets: Observations and modelling

James D. Kirkham [a, b, *], Kelly A. Hogan [a], Robert D. Larter [a], Neil S. Arnold [b], Jeremy C. Ely [c], Chris D. Clark [c], Ed Self [d], Ken Games [d], Mads Huuse [e], Margaret A. Stewart [f], Dag Ottesen [g], Julian A. Dowdeswell [b]

[a] British Antarctic Survey, High Cross, Madingley Road, Cambridge, CB3 0ET, UK
[b] Scott Polar Research Institute, University of Cambridge, Cambridge, CB2 1ER, UK
[c] Department of Geography, The University of Sheffield, Sheffield, UK
[d] Gardline Limited, Hewett Road, Great Yarmouth, NR31 0NN, UK
[e] School of Earth and Environmental Sciences, University of Manchester, Manchester, M13 9PL, UK
[f] British Geological Survey, The Lyell Centre, Research Avenue South, Edinburgh, EH14 4AP, UK
[g] Geological Survey of Norway, P.O. Box 6315 Torgarden, N-7491 Trondheim, Norway

ARTICLE INFO

Article history:
Received 30 March 2022
Received in revised form
18 July 2022
Accepted 25 July 2022
Available online xxx

Handling Editor: Dr C. Ó Cofaigh

Keywords:
Tunnel valley
Meltwater
Deglaciation
3D seismic-reflection data
Ice sheets
North sea

ABSTRACT

The geological record of landforms and sediments produced beneath deglaciating ice sheets offers insights into inaccessible glacial processes. Large subglacial valleys formed by meltwater erosion of sediments (tunnel valleys) are widespread in formerly glaciated regions such as the North Sea. Obtaining a better understanding of these features may help with the parameterisation of basal melt rates and the interplay between basal hydrology and ice dynamics in numerical models of past, present, and future ice-sheet configurations. However, the mechanisms and timescales over which tunnel valleys form remain poorly constrained. Here, we present a series of numerical modelling experiments, informed by new observations from high-resolution 3D seismic data (6.25 m bin size, ~4 m vertical resolution), which test different hypotheses of tunnel valley formation and calculate subglacial water routing, seasonal water discharges, and the rates at which tunnel valleys are eroded beneath deglaciating ice sheets. Networks of smaller or abandoned channels, pervasive slump deposits, and subglacial landforms are imaged inside and at the base of larger tunnel valleys, indicating that these tunnel valleys were carved through the action of migrating smaller channels within tens of kilometres of the ice margin and were later widened by ice-contact erosion. Our model results imply that the drainage of extensive surface meltwater to the ice-sheet bed is the dominant mechanism responsible for tunnel valley formation; this process can drive rapid incision of networks of regularly spaced subglacial tunnel valleys beneath the fringes of retreating ice sheets within hundreds to thousands of years during deglaciation. Combined, our observations and modelling results identify how tunnel valleys form beneath deglaciating mid-latitude ice sheets and have implications for how the subglacial hydrological systems of contemporary ice sheets may respond to sustained climate warming.

1. Introduction

Subglacial hydrology exerts a major control on ice-sheet dynamics, sedimentation rates, and landscape evolution. Currently, mass losses from the Antarctic and Greenland ice sheets are accelerating (Shepherd et al., 2018, 2020; Mouginot et al., 2019; Rignot et al., 2019). Increasing numbers of lakes on the surface of the Greenland Ice Sheet are forming further inland (Leeson et al., 2015; Gledhill and Williamson, 2017). These lakes can drain, sometimes rapidly (e.g., Zwally et al., 2002; Das et al., 2008; Selmes et al., 2011; Smith et al., 2015; Chudley et al., 2019), transporting great quantities of meltwater to the base of the ice sheet. Widespread melting events have also been observed around the fringes of the Antarctic Ice Sheet and these are predicted to increase in

* Corresponding author. British Antarctic Survey, High Cross, Madingley Road, Cambridge, CB3 0ET, UK.
E-mail address: jk675@cam.ac.uk (J.D. Kirkham).

https://doi.org/10.1016/j.quascirev.2022.107680

extent in the future (Scambos et al., 2000; Tedesco, 2009; Tedesco and Monaghan, 2009; Trusel et al., 2015; Kingslake et al., 2017; Bell et al., 2018). Subglacial hydrology will play an increasingly important role in the fate and behaviour of these ice sheets as the climate continues to warm. However, the subglacial hydrological system is highly inaccessible, and models of how the subglacial drainage system of contemporary ice sheets will adapt to future climate warming are poorly constrained. Consequently, there is great value in examining what we can learn about subglacial hydrology from the demise of former ice sheets.

Some of the most striking landforms associated with subglacial meltwater in formerly glaciated regions take the form of elongate depressions known as tunnel valleys. Tunnel valleys typically form on low relief beds near former ice-sheet margins and can be incised into both unlithified sediments and bedrock (Kehew et al., 2012; van der Vegt et al., 2012; Livingstone and Clark, 2016). They are commonly hundreds to thousands of metres wide, tens to hundreds of metres deep and form semi-regularly spaced channel networks with spacings of ~2–9 km (Kehew et al., 2012; van der Vegt et al., 2012; Livingstone and Clark, 2016; Ottesen et al., 2020). Tunnel valleys are ubiquitous deglacial landforms which are observed frequently in the geological record in both the Quaternary (e.g., Woodland, 1970; Wright, 1973; Mooers, 1989; Praeg, 1996; Huuse and Lykke-Andersen, 2000; Kristensen et al., 2007; Müther et al., 2012; Stewart et al., 2012; Moreau and Huuse, 2014; Montelli et al., 2020) and pre-Quaternary glacial periods (e.g., Ghienne and Deynoux, 1998; Hirst et al., 2002; Le Heron et al., 2004; Douillet et al., 2012; Montelli et al., 2019). They can transport large quantities of water and sediment (Livingstone and Clark, 2016) and may play a critical role in regulating ice-stream stability during deglaciation by draining meltwater away that might otherwise have reduced basal friction and increased basal sliding (Lelandais et al., 2018). The termini of tunnel valleys are often used as markers to locate the position of former ice margins (e.g., Wingfield, 1989; Huuse and Lykke-Andersen, 2000; Sandersen et al., 2009; Lohrberg et al., 2020; Ottesen et al., 2020). In some regions, multiple generations of buried cross-cutting tunnel valleys exist; information from which may be used to reconstruct the history of glaciations that occurred prior to the last glacial period (Jørgensen and Sandersen, 2006; Kristensen et al., 2007; Stewart and Lonergan, 2011; Douillet et al., 2012; Atkinson et al., 2013; Stewart et al., 2013; Pugin et al., 2014; Montelli et al., 2020).

Although the origin of tunnel valleys has been attributed to erosion by pressurised subglacial meltwater for over 100 years (Jentzsch, 1884; Ussing, 1903, 1907), the rates at which they form, the processes involved and their impact on ice-sheet dynamics are still subjects of intense debate (Ó Cofaigh, 1996; Huuse and Lykke-Andersen, 2000; Kehew et al., 2012; van der Vegt et al., 2012). Theories explaining tunnel valley formation can be broadly divided into two genetic models: formation through (i) 'outburst' flooding and (ii) 'gradual' or 'seasonal' incision by relatively small water fluxes (e.g., Ó Cofaigh, 1996; Praeg, 1996; Kehew et al., 2012; van der Vegt et al., 2012, Fig. 1).

Due to their large dimensions and extensive geographical distribution, many authors have suggested that large volumes of water must have been involved in tunnel valley formation. This has led to a proposed mechanism in which outburst floods from trapped, subglacially stored reservoirs erode large volumes of material rapidly under high discharges (e.g., Wright, 1973; Wingfield, 1990; Piotrowski, 1994; Cutler et al., 2002; Jørgensen and Sandersen, 2006). The water reservoirs for these floods may reside in subglacial basins or be trapped behind frozen toes of permafrost near the ice margin, releasing water as the ice edge retreats (Fig. 1A; Piotrowski, 1994).

The magnitude of flooding, or the number of flood repetitions required for tunnel valley genesis, is not well constrained. Repeated low to moderate magnitude floods that reoccupy the same narrow meltwater pathway, potentially during multiple glaciations, have been offered as an explanation for the superposition of smaller channel infill structures within larger tunnel valley tracts (Jørgensen and Sandersen, 2006; Sandersen et al., 2009). In contrast, much larger discharges capable of forming entire networks of tunnel valleys in massive sheet floods have also been proposed (e.g., Shaw and Gilbert, 1990; Brennand and Shaw, 1994) but this hypothesis is not widely accepted due to the enormous quantities of water required and absence of supporting evidence in the distal sedimentary record (Ó Cofaigh, 1996).

The alternative group of hypotheses proposed to explain tunnel valley formation build around the concept that tunnel valleys are formed incrementally by meltwater flowing under steady-state conditions rather than catastrophically, allowing their extensive incisions to build up time-transgressively. Theories comprising this hypothesis focus around the seasonal propagation of surface meltwater to the bed through an efficient supra-to-subglacial drainage system connection (Fig. 1B), or sediment creep into a low pressure channel driven by high basal porewater pressures alone (Fig. 1C). Both of these mechanisms imply that meltwater pathways remained relatively stable in space in order for smaller water discharges to gradually incise a large tunnel valley, potentially aided by the enlargement of the upper valley cross section by ice (Huuse and Lykke-Andersen, 2000; Kehew et al., 2012; van der Vegt et al., 2012). Pervasive slumping of the tunnel valley flanks may also have enhanced the lateral expansion of the tunnel valleys (Prins et al., 2020; Kirkham et al., 2021).

In the sediment-creep hypothesis (e.g., Shoemaker, 1986; Boulton and Hindmarsh, 1987; Mooers, 1989), headward erosion of a small conduit by piping is triggered in response to increased porewater pressures caused by insufficient evacuation of meltwater from the subglacial environment (Fig. 1C). As fluid pressures within the conduit are lower than in the surrounding bed, groundwater flows towards the conduit via steady-state Darcian flow, causing the conduit to enlarge into a tunnel valley as sediment is eroded from the channel walls (Boulton and Hindmarsh, 1987). Once established, the conduit may tap into upstream subglacial lakes, further enlarging the channel through outburst flooding (Hooke and Jennings, 2006).

Alternatively, the seasonal input of supraglacial, rather than basal, meltwater to the bed of the ice sheet may gradually incise tunnel valleys (Fig. 1B). Analogues from the present-day Greenland Ice Sheet demonstrate that large volumes of meltwater are mobilised during the ablation season; these are transported to the bed through connections such as moulins and crevasses on the ice-sheet surface (Bartholomew et al., 2011; Tedesco et al., 2013; Smith et al., 2015; Banwell et al., 2016; Koziol et al., 2017; Koziol and Arnold, 2018). Similar, and probably even more extensive, surface-to-bed hydraulic connections were likely present across the surface of former mid-latitude ice sheets as they deglaciated, providing a water source to facilitate tunnel valley incision.

The steady-state body of hypotheses require less specific circumstances than the 'outburst flood' hypotheses, such as not needing to invoke large subglacial lakes or permafrost trapping of water. Thus, this formative mechanism is appealing given the widespread geographical distribution of tunnel valleys (Kehew et al., 2012; van der Vegt et al., 2012). Nevertheless, steady-state formation hypotheses have often been disregarded because of the assumption that channels hundreds of metres deep and kilometres wide must require huge discharges in order to form rapidly. However, recent research utilising numerical models of erosion from subglacial water flow and stratigraphic investigations has challenged both of these assumptions.

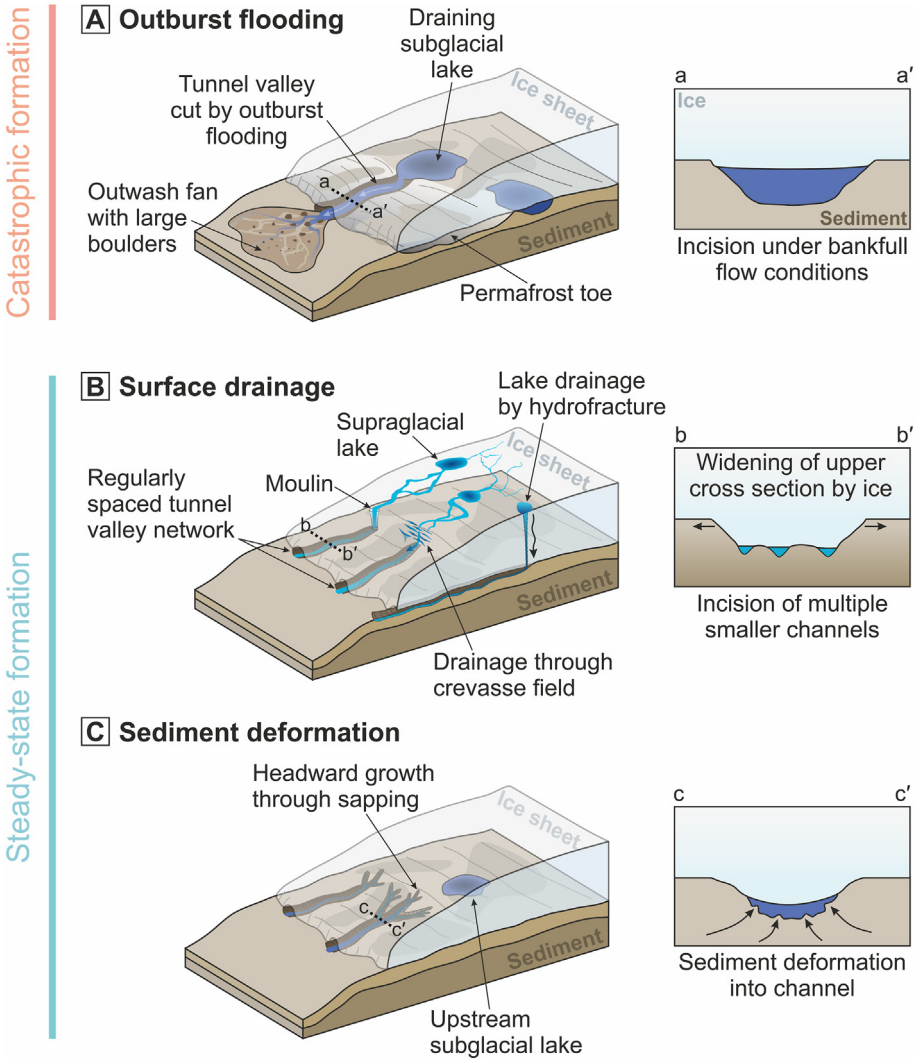

Fig. 1. Previously proposed mechanisms of tunnel valley formation. (A) Catastrophic formation via outburst flooding from subglacial lakes trapped behind a frozen toe of permafrost. High water discharges and bankfull flow conditions result in the deposition of an outwash fan containing large boulders at the ice-sheet terminus. **(B)** Steady-state formation close to the ice margin, with water sourced from surface melting, resulting in the formation of regularly spaced tunnel valley networks. Surficial streams drain meltwater to the ice-sheet bed where smaller channels, possibly arranged in a braided structure, gradually incise a larger valley. **(C)** Gradual headward growth by sapping, possibly towards subglacial lakes trapped upstream. Tunnel valleys grow as sediment deforms into the low pressure channel, and sediment is removed by the transport of meltwater towards the ice-sheet terminus.

Sandersen et al. (2009) used lithological and biostratigraphical data from northern Denmark to constrain the age of tunnel valleys formed during the recession of the Late Weichselian Eurasian Ice Sheet across this region. The tunnel valleys were incised during temporary stillstands of the retreating ice-sheet margin between ~19 ka and 18 ka, leaving only a few hundred years at each ice-margin position for the features to form (Sandersen et al., 2009). The formation of a series of ~1–2 km wide, 5–10 km long and up to 180 m deep valleys within a few hundred years demonstrates rapid incision of the tunnel valleys near the ice-sheet margin. Similarly, Giglio et al. (2021) inferred that the maximum time available to carve an extensive system of tunnel valleys into lithified bedrock in the Celtic Sea during the last glacial period was ~1–2 kyrs. Erosive meltwater drainage occurred concurrently with a period of rapid retreat of the Irish Sea Ice Stream across the continental shelf (Giglio et al., 2021). These studies provide observational benchmarks against which theories of tunnel valley formation can be tested.

Sandersen et al. (2009) invoked repeated outbursts of meltwater along narrow conduits to explain the rapid formation of the tunnel valleys in northern Denmark. However, recent numerical modelling by Beaud et al. (2018) suggests that small-magnitude discharge events in the form of seasonal influxes of meltwater from the ice-sheet surface can excavate large channels (100s m wide and 10s m deep) into bedrock over thousands of years (Beaud et al., 2016, 2018). Whilst their model is applicable only to the erosion of bedrock channels, and different governing equations would be needed to test these findings on poorly consolidated sediments (e.g., Walder and Fowler, 1994), these model results challenge the assumption that high-magnitude subglacial discharges are necessary to erode large tunnel valleys rapidly beneath the margins of deglaciating ice sheets. The results of Sandersen et al. (2009) and Beaud et al. (2018) warrant further investigation of the minimum seasonal meltwater discharges required to erode tunnel valleys into poorly consolidated sediments over hundreds of years. This will help to establish which formation process is most likely, and may elucidate the impact that tunnel valley formation has on ice-sheet dynamics (van der Vegt et al., 2012).

In this study, we attempt to answer these questions using an ice-sheet modelling approach informed by new geomorphological observations from high-resolution 3D seismic analyses of tunnel valley morphology. We quantify possible water fluxes and erosion rates beneath deglaciating ice sheets and use these calculations to test previously proposed hypotheses of tunnel valley formation.

2. Methods

In this study, we simulate subglacial water fluxes and routing beneath the last British-Irish and Fennoscandian ice sheets to provide greater understanding of tunnel valley formation in the North Sea. It is important to note that the tunnel valleys present in this region are largely attributed to glaciations which occurred prior to the last glacial period (particularly the Elsterian Glaciation; 430–450 ka), although some examples from the last glacial period do exist (e.g., Sandersen et al., 2009; Giglio et al., 2021). We deliberately choose to focus on modelling water flow during the last glacial period because the ice-sheet geometries and climate forcings are considerably better constrained than those of earlier glaciations (e.g., Svendsen et al., 2004; Batchelor et al., 2019; Gowan et al., 2021). Accordingly, this study does not aim to provide a realistic representation of the water routing beneath the ice sheets that formed the majority of tunnel valleys in this region. Instead, we assume that the ice sheets present during the last glacial period can provide physically plausible constraints on the ice-sheet geometries and climatic conditions experienced during previous glaciations when most tunnel valleys formed. We use these relatively well-constrained boundary conditions to quantify a realistic range of water fluxes, melt rates and timescales of channel incision which inform about processes of tunnel valley formation.

2.1. Detailed channel morphology from high-resolution 3D seismic data

We frame our water routing and erosion modelling experiments in the context of detailed geomorphological observations derived from high-resolution 3D (HR3D) seismic data. HR3D seismic data are capable of revealing intricate morphological details of buried landforms and deposits, many of which cannot be resolved using conventional 3D seismic methods (Kirkham et al., 2021). These previously unseen details provide new insights into incision processes, realistic water fluxes and the mode of meltwater drainage within the tunnel valleys.

We examined seven HR3D seismic datasets in the central North Sea (Fig. 2; Kirkham et al., 2021) covering a combined area of ~67 km^2 and containing a total of 23 tunnel valleys. The acquisition system comprised two 1200-m-long streamers towed 3 m beneath the sea surface with 96 hydrophone groups at 12.5 m spacing, a 6.25 m shot interval and a 1-ms sample rate (Games, 2012). The seismic source was two 160-in^3 (2.62 L) sleeve airgun clusters. Data processing included swell noise attenuation, tide correction,

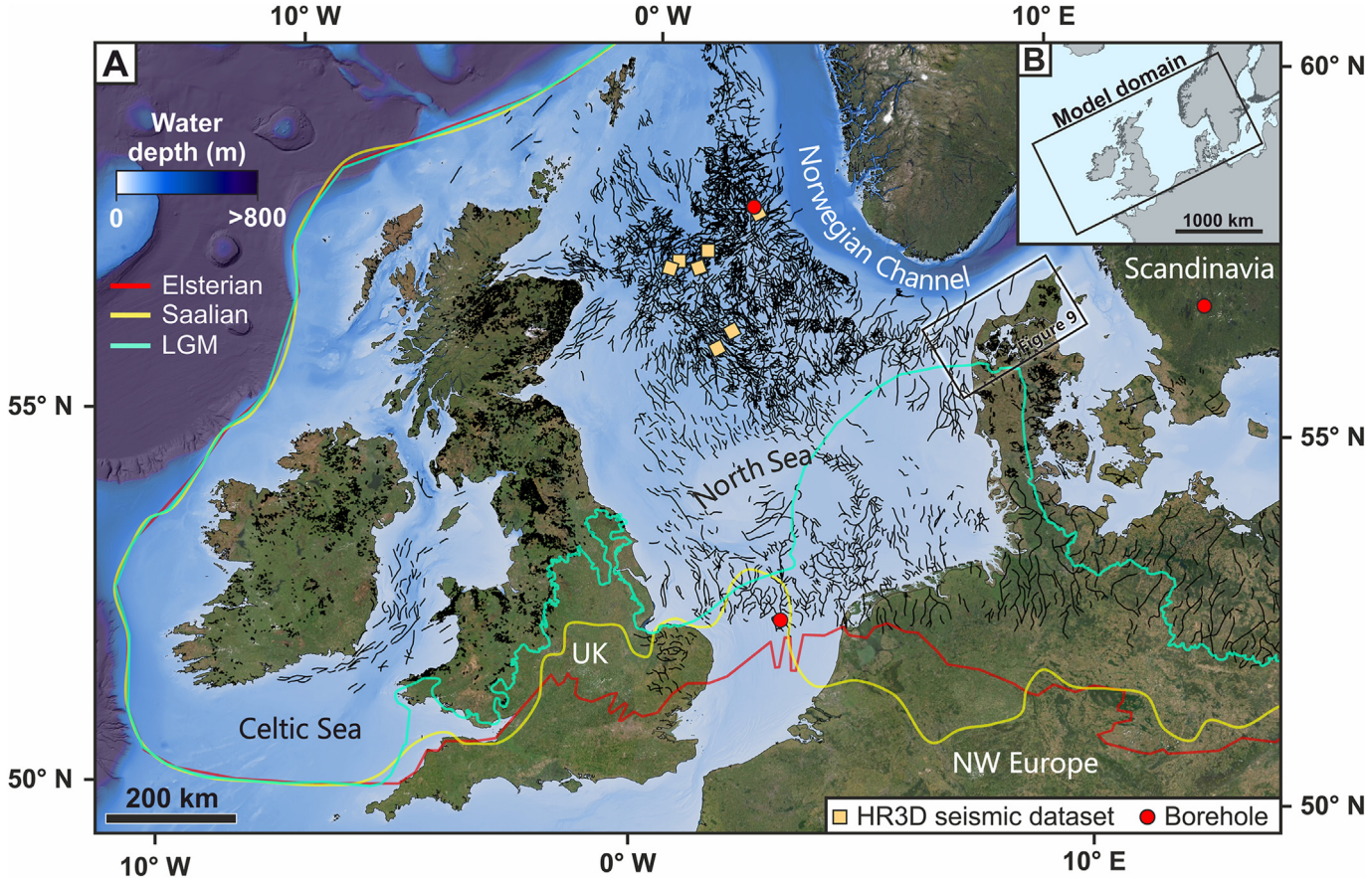

Fig. 2. Study area. (A) Distribution of tunnel valleys in the North Sea and surrounding landmasses (van der Vegt et al., 2012; Ottesen et al., 2020), and meltwater channels on the UK mainland (Clark et al., 2018), in relation to the high-resolution 3D (HR3D) seismic datasets (orange squares) and boreholes (red circles) used in this study. Best estimate former ice margin positions for the Last Glacial Maximum (LGM), Saalian Glaciation (MIS 6), and Elsterian Glaciation (MIS 12) are shown from Batchelor et al. (2019). Regional bathymetry is from GEBCO (https://www.gebco.net). **(B)** Extent of the modelling domain used in this study. (For interpretation of the references to colour in this figure legend, the reader is referred to the Web version of this article.)

multiple suppression, two passes of velocity analysis run at 250 × 250 m intervals, normal-moveout correction, bandpass filtering (20–250 Hz), stacking, and migration. The final processed datasets consist of time-migrated 3D stacks with a 1-ms sample rate, a 6.25 × 6.25 m bin size, a vertical resolution of ~4 m, and a detection limit for depth changes along individual reflectors of ~0.5 m (King, 2020; Kirkham et al., 2021).

The base, sides, and internal fill packages of each tunnel valley were mapped and laterally traced through the HR3D seismic volumes using S&P Global Kingdom Software. Picking of seismic horizons was largely conducted manually on a seismic line-by-line basis because automated picking algorithms struggled to follow the complex tunnel valley shapes. The mapped tunnel valley seismic horizons were converted from two-way travel time (TWT) to depth using a velocity of 1900 m s^{-1}, which is appropriate for the Pleistocene sediments in this region (Kristensen and Huuse, 2012). Characteristic morphological measurements such as width, depth and cross-sectional area were then derived for each tunnel valley.

2.2. Modelling subglacial water flux and routing

2.2.1. BRITICE-CHRONO ice sheet modelling data

The geometry, thickness, surface slope, and the basal and surface melt rates of the last British-Irish Ice Sheet were derived from a series of palaeo ice-sheet reconstructions produced using the Parallel Ice Sheet Model (PISM) as part of the BRITICE-CHRONO project (Clark et al., 2021; Clark et al., In review). PISM is a three-dimensional, thermomechanical ice-sheet model constrained by geological observations which combines shallow-ice and shallow-shelf approximations for grounded ice to capture dynamic ice behaviour (Winkelmann et al., 2011). The model was run at a high horizontal resolution of 5 km, with a domain which covers the British Isles and parts of Scandinavia (Fig. 2B), to capture the interaction between the British-Irish and Fennoscandian ice sheets.

Climate was prescribed using the glacial index method (e.g., Marshall et al., 2000; Tarasov and Peltier, 2004; Zweck and Huybrechts, 2005; Niu et al., 2019), whereby climate was scaled along the Greenland ice core record between different 1 kyr climate reconstructions derived from the PMIP3 simulations and palaeogeographical maps (Clark et al., In review). Temperature and precipitation from the index approach were converted into surface mass balance through a positive degree day model. For areas of the ice sheet with a negative surface mass balance, the mass balance values were converted into surface melt rates and added to the steady-state basal melt rate derived from geothermal and frictional strain heating (Cuffey and Paterson, 2010). Geothermal heat flux varied spatially and was compiled from data collected by the British Geological Survey and Geological Survey Ireland (see Gandy et al., 2019). This combined melt rate was then used to calculate the subglacial water flux at each grid cell. Following widespread observations of surface meltwater draining to the base of the modern-day Greenland Ice Sheet (e.g., Bartholomew et al., 2011; Andrews et al., 2014; Smith et al., 2015; Banwell et al., 2016; Koziol et al., 2017; Nienow et al., 2017), we make a first-order assumption that all surface melt water propagates to the bed of the ice sheet, rather than flowing to the margin in supraglacial streams, for the deglacial scenarios considered here. We justify this assumption given the very high proportion of surface runoff that was observed to enter the subglacial hydrological system of the contemporary Greenland Ice Sheet through moulins fed by supraglacial streams during an extreme melt event in 2012 (Smith et al., 2015); conditions that may be analogous to the meltwater transport regime experienced during deglaciation.

Model outputs were taken at four timeslices (27 ka, 21 ka, 19 ka, and 18 ka) to investigate changes in subglacial discharge and water routing as the last British-Irish and Fennoscandian ice sheets deglaciated. Modern topography of the North Sea and surrounding landmasses was taken from the EMODnet digital bathymetry dataset (EMODnet Bathymetry Consortium, 2018), which has a grid spacing of ~115 m. These modern topographic data were corrected for isostasy by applying the results of a new glacial isostatic adjustment model of the British Isles and northwest Europe that is constrained by geomorphological and geochronological data collated by the BRITICE-CHRONO consortium, the DATED-1 project, and a recently updated regional sea-level database for the last 20 kyr (Bradley et al., 2018). The model accounts for far field sea-level effects (e.g., gravitational attraction, different glacial histories) and near field ice loading.

2.2.2. Subglacial water routing

Water routing over the ~2,750,000 km^2 model domain was modelled using an upstream area algorithm (Arnold, 2010) that has been adapted for subglacial water routing (e.g., Willis et al., 2016; Kirkham et al., 2019). The direction that water is routed beneath ice masses is controlled by gradients of subglacial hydraulic potential (Shreve, 1972). The subglacial hydraulic potential, φ, of water flowing beneath an ice sheet is a function of bed topography and ice thickness:

$$\varphi = \rho_w g h + k \rho_i g Z \quad (1)$$

where ρ_w and ρ_i are the densities of water and ice (kg m^{-3}), respectively, g is the acceleration due to gravity (m s^{-2}), h is bed elevation (m), Z is ice thickness (m) and k is a dimensionless parameter (referred to as the uniform floatation factor) that represents the ratio between subglacial water pressure and ice overburden pressure (Table 1). The value of k varies both spatially and temporally depending on the quantity of meltwater input from the surface, basal ice temperature, the character of the subglacial drainage system and the properties of the underlying substrate (Shreve, 1972; Andrews et al., 2014). In this study, we employ a k-value of 0.925. This value has been shown to be realistic when averaged over an entire melt-season, according to empirical studies from several sectors of the Greenland Ice Sheet (Banwell et al., 2013; Lindbäck et al., 2015), and has been used previously to model water flow beneath the former Scandinavian and Barents Sea ice sheets (Shackleton et al., 2018).

The routing algorithm passes the cumulative subglacial water flux, derived from the sum of surface and basal melting from the ice-sheet model, downstream from cell to cell until the routing algorithm reaches the edge of the digital elevation model (DEM). This allows the direction and the steady-state subglacial water discharge in each DEM cell to be calculated (Arnold, 2010; Willis et al., 2016). Subglacial water routing across the isostatically corrected bed of the former ice-sheet complex was conducted at a 1500-m resolution, whilst detailed model runs used for calculating tunnel valley erosion rates (Section 2.3) were conducted around the fringes of the ice sheet at a 50-m resolution.

2.2.3. Tunnel valley carrying capacity

In addition to calculating the steady-state discharges resulting from basal and surface melting, we calculate the maximum carrying capacity of the tunnel valleys based on their cross-sectional area (Walder, 1986; Wingham et al., 2006; Jordan et al., 2010). The maximum discharge capable of being carried by a channel, Q_{max} (m^3 s^{-1}), is equal to:

Table 1
Definitions, values and sources of parameters used throughout the text.

Symbol	Parameter	Value [units]	Source
α_{cc}	Channel geometry factor	5500–233,000 [unitless]	Carter et al. (2017); HR3D seismic measurements
$\bar{c}$	Sediment concentration in water	1500 mg L^{-1}	Observations from flood stage rivers (Williams, 1989)
$\dot{D}$	Deposition rate	[m s^{-1}]	Model output
D_{15}	15th percentile grain size	0.01–0.1 mm	Borehole measurements; Fig. 3
$\dot{E}$	Erosion rate	[m s^{-1}]	Model output
f_{cc}	Channel roughness parameter	0.07 $m^{-2/3}$ s^{-2}	Carter et al. (2017)
g	Acceleration due to gravity	9.81 m s^{-2}	Constant
h	Bed elevation	[m]	BRITICE-CHRONO model output (EMODnet Bathymetry Consortium and Consortium, 2018)
k	Uniform floatation factor	0.925 [unitless]	(Banwell et al., 2013; Lindbäck et al., 2015; Shackleton et al., 2018)
K_1	Erosion constant	0.1 [unitless]	Walder and Fowler (1994)
K_2	Deposition constant	6 [unitless]	Walder and Fowler (1994)
m	Manning coefficient	0.025 $m^{-1/3}$ s	Constant
p_i	Density of ice	918 kg m^{-3}	Constant
p_s	Density of sediment	2150 kg m^{-3}	Borehole measurements
p_w	Density of water	1000 kg m^{-3}	Constant
Q_{max}	Maximum tunnel valley carrying capacity	[m^3 s^{-1}]	Calculated
S	Channel cross-sectional area	[m^2]	HR3D seismic measurements
τ_{cc}	Channel bed shear stress	[Pa]	Calculated
τ_k	Critical shear stress	[Pa]	Calculated
u_c	Channel flow velocity	[m s^{-1}]	Water routing model output
μ_w	Viscosity of water	1.78 x 10^{-3} Pa s	Constant
v_s	Mean sediment settling velocity	[m s^{-1}]	Calculated
Z	Ice thickness	[m]	BRITICE-CHRONO model output
φ	Hydraulic potential	[Pa]	Calculated from BRITICE-CHRONO model output
φ'	Hydraulic potential gradient	[Pa m^{-1}]	Calculated from BRITICE-CHRONO model output

$$Q_{max} = 2\left(\frac{\pi}{2}\right)^{\frac{1}{3}} S^{\frac{4}{3}} m^{-1} \left(\frac{\varphi'}{p_w g}\right)^{\frac{1}{2}} \quad (2)$$

where S is the cross-sectional area (m^2) of a channel, φ' is the hydraulic potential gradient, and m is the Manning coefficient ($m^{-1/3}$ s) describing the internal roughness of the channel. Representative channel cross-sectional areas were derived from measurements of a selection of tunnel valleys imaged in the HR3D seismic-reflection data.

2.3. Modelling tunnel valley erosion

2.3.1. Erosion model

To better constrain the fluxes of water and the time required to incise tunnel valleys downwards into poorly consolidated sediments, like those of the North Sea Basin (e.g., Ziegler, 1990; Huuse and Lykke-Andersen, 2000; Lamb et al., 2018), we apply a model of subglacial channel erosion into a deformable substrate developed by Carter et al. (2017), based on the work of Walder and Fowler (1994). This model has been used previously to simulate the formation of channels through subglacial lake drainage beneath the Antarctic Ice Sheet (Carter et al., 2017), and to estimate incision rates of large subglacial channels in the Green Bay Lobe, Wisconsin, during the last glacial period (Zoet et al., 2019). The model calculates the balance between the water-driven erosion of the base and walls of a soft-bedded subglacial channel and the sediment deposition rate within the channel, estimated using Stokes' settling law (Walder and Fowler, 1994). A viscous substrate rheology was invoked in Walder and Fowler (1994) and Carter et al. (2017) to simulate till flux into the channel, which acts to offset a portion of the mass loss due to water erosion. However, this rheology is inconsistent with laboratory data, numerical experiments and field studies (e.g., Iverson et al., 1998; Tulaczyk et al., 2000a, 2000b; Iverson et al., 2007; Damsgaard et al., 2017; Zoet and Iverson, 2020). Accordingly, we follow Zoet et al. (2019) and omit the viscous portion of the model here.

The erosion rate (m s^{-1}), $\dot{E}$, of a sedimentary channel is calculated as:

$$\dot{E} = K_1 \left(\frac{v_s}{\alpha_{cc}}\right)\left(\frac{\max(\tau_{cc} - \tau_k, 0)}{g(\rho_s - \rho_w)D_{15}}\right)^{\frac{3}{2}} \quad (3)$$

where v_s is the mean sediment settling velocity, K_1 is an erosion constant (Walder and Fowler, 1994), τ_{cc} is the channel bed shear stress, τ_k is the critical shear stress at the base of the channel, D_{15} is the 15th percentile grain-size diameter of the sediments carried within the flowing water, ρ_s is the density of sediment, ρ_w is the density of water, and α_{cc} is a channel geometry correction factor which can be approximated as (width/depth)^3 (Carter et al., 2017). We derive α_{cc} from measurements from our HR3D seismic data, and investigate a range of D_{15} values guided by the grain-size distribution of tunnel valley infill sediments sampled from boreholes in the North Sea and western Europe (Figs. 2 and 3; Benvenuti et al., 2018; Peterson et al., 2018).

The rate of sediment deposition within the channel, $\dot{D}$ (m s^{-1}), is:

$$\dot{D} = K_2 \frac{v_s}{\alpha_{cc}} \bar{c} \sqrt{\frac{gD_{15}(\rho_s - \rho_w)}{\tau_{cc}}} \quad (4)$$

where K_2 is a deposition constant (Walder and Fowler, 1994) and $\bar{c}$ is the sediment concentration in subglacial waters which, following Zoet et al. (2019), we estimate from measurements of sediment concentrations in flood-stage rivers (Williams, 1989).

Following Carter et al. (2017), τ_{cc}, τ_k, and v_s are estimated as:

$$\tau_{cc} = \left|\frac{1}{8} f_{cc} \rho_w {u_c}^2\right| \quad (5)$$

$$\tau_k = 0.025 D_{15} g(\rho_s - \rho_w) \quad (6)$$

$$v_s = {D_{15}}^2 \frac{2(\rho_s - \rho_w)g}{9\mu_w} \quad (7)$$

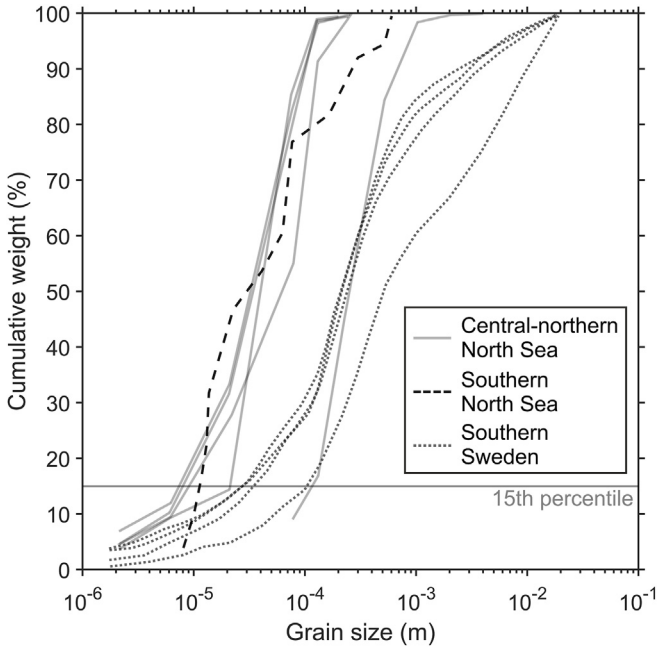

Fig. 3. Distribution of grain sizes from boreholes drilled into the infill of tunnel valleys in the central-northern North Sea, the southern North Sea (Benvenuti et al., 2018), and southern Sweden (Peterson et al., 2018). See Fig. 2A for borehole locations. The horizontal grey line indicates the 15th percentile of grain size used as a model parameter (D_{15}) in the water erosion simulations. The grain-size distributions for tunnel valleys in the central-northern North Sea were derived from geotechnical boreholes acquired in an area of HR3D seismic data coverage.

where f_{cc} is a channel roughness parameter (Carter et al., 2017), u_c is the channel water velocity and μ_w is the viscosity of water.

Many of the parameters governing the balance between erosion and deposition within the tunnel valleys can be constrained from the HR3D seismic data or from boreholes drilled into the tunnel valleys (Table 1), increasing our confidence in the calculated values of $\dot{E}$ and $\dot{D}$. Nonetheless, some of our model parameters remain loosely constrained and thus we treat these rates as order of magnitude estimates to assess the likely timescales in which tunnel valleys form.

2.3.2. *Testing scenarios of tunnel valley formation: outburst floods versus steady seasonal melt supply*

We test two scenarios of tunnel valley formation by varying the magnitude and duration of meltwater input into the erosion model:

(i) Outburst flooding: we use the hydrograph from the 1938 jökulhlaup at Grímsvötn (Björnsson, 1992) to simulate the erosive impact of a short, high magnitude outburst flood spread across a wide (500-m or 1000-m) channel. This flooding event released ~4 km^3 of water over ~10 days, attaining peak discharges of ~20,000 $m^3\ s^{-1}$. We also upscale this flood hydrograph to simulate the drainage of a larger 15-km^3 lake over the same time period, attaining peak flow discharges of ~80,000 $m^3\ s^{-1}$. These hydrographs represent some of the largest subglacial floods documented in observational records (Gudmundsson et al., 1995; Björnsson, 2002).

(ii) Seasonal surface drainage: total annual surface melt, added to the steady-state basal melt rate from geothermal and frictional strain heating (~0.01–0.06 m yr^{-1}), is input over a 4-month period to mimic the seasonal input of surface meltwater to the ice-sheet bed over an ablation season, such as is observed on the contemporary Greenland Ice Sheet (e.g., Banwell et al., 2016; Koziol and Arnold, 2018). When input into the subglacial hydrological system, water is routed within smaller 100-m wide channels.

We apply the erosion model to the areas of the ice sheet that experienced surface melting and assume that all supraglacial meltwater propagates to the bed for the seasonal drainage scenario. Although surface meltwater can propagate to the bed through a variety of mechanisms which operate at different rates such as hydrofracturing, seasonally open moulins or through crevasses, we account for these processes in a simplified way by inputting surface meltwater at individual grid cells randomly distributed across the area where surface melting is predicted to occur. These input cells essentially operate as synthetic moulins distributed across the ice-sheet surface. The volume of surface meltwater input through each moulin is scaled so that moulins in areas of more negative surface mass balance receive a higher proportion of the total surface melt. For the seasonal scenario, a moulin density of 0.2 km^{-2} was chosen based on the observed distribution of moulins on the ablation zone of present-day Greenland during the summer melt season (Zwally et al., 2002; Colgan and Steffen, 2009; Banwell et al., 2016). Sensitivity of the model to moulin density was tested using densities of 0.05–0.8 km^{-2}; however, this parameter was found to have little impact on the overall magnitude of subglacial discharge downstream (discharge typically varied by ±12–20%, partly due to the randomised placement of moulins).

Our modelling approach assumes that the British-Irish and Fennoscandian ice sheets underwent substantial surface melting during deglaciation. This assumption is justified because modelled deglacial mass balances around the ice-sheet fringes are negative and are of the same order of magnitude as those recorded from regions of present-day Greenland where substantial surface melt features are known to drain to the bed (e.g., Zwally et al., 2002; Das et al., 2008; Colgan and Steffen, 2009; Selmes et al., 2011; Leeson et al., 2015; Chudley et al., 2019; Mouginot et al., 2019).

A nested modelling approach was taken whereby subglacial water fluxes resulting from basal melting within the interior of the ice sheet were first calculated at a 1500-m resolution. The steady-state discharges resulting from basal melt were then input to the edges of a high-resolution 50-m grid covering the ice-sheet ablation zone. Subglacial discharges generated from basal melting were added to the water input derived from surface melt and routed through the finer-scale grid. The resulting subglacial discharges were then used to calculate tunnel valley erosion rates using equations (3) and (4). Water inputs from surface melting were typically 3–5 orders of magnitude greater than those from basal melting in the ablation zone of the ice sheet.

We chose to conduct a high-resolution (50-m grid) water routing case study over northern Denmark as the chronology of Weichselian tunnel valley incision is well constrained there (Sandersen et al., 2009). This chronological information allows us to test the different models of tunnel valley formation and to investigate which mechanism can achieve the rapid incision rates inferred for 18–19 ka (Sandersen et al., 2009). An initial model run was conducted to assess broad-scale water routing pathways. We assume that water routed along these pathways will erode channels over time (concurrent with palaeo observations; e.g., Mooers, 1989; Praeg, 1996; Kehew et al., 2012), and define the maximum length of the channels as the limit at which channelised subglacial discharge no longer exceeds 20 times the average value of the neighbouring cells. Artificial channels with specified widths of 100 m, 500 m and 1000 m were then incised by ~30 m into the isostatically-corrected bed topography. These depressions route the majority of the input meltwater into these channels, allowing us to

calculate erosion rates within the channels and to test different formation hypotheses relating to water discharge, flow duration and channel size.

3. Results

3.1. Tunnel valley morphology and discharge

The seven HR3D datasets from the North Sea image 23 cross-cutting elongate incisions, previously interpreted as tunnel valleys (Kirkham et al., 2021). The tunnel valleys are 300–3000 m wide, up to 300 m deep, 10,000–100,000 m^2 in cross-sectional area, with typical side slopes of 15–40°. The valleys are generally 5–10 times wider than they are deep. Many tunnel valleys are characterised by a narrow V-shaped base and a wider upper cross section (Fig. 4A). Terraces are sometimes present adjacent to the boundary of the V-shaped incision. Several tunnel valleys also contain chaotic and displaced reflections at their sides and bases, which correspond to slumping and faulting along the sides of the features (Fig. 4B). Where present, the slumps constitute between ~8 and 41% of the tunnel valley infill by cross-sectional area and have slope angles at their outer boundaries of 10–42°.

The mass movements present within the tunnel valleys are sometimes associated with subtle curvilinear ridges which appear as distinct anomalies in seismic coherence attribute analyses (Fig. 5A and B). The ridges have symmetrical cross-sections, are often cuspate or sinuous in form, and run parallel to the tunnel valley edges. Two subsets of ridge types are identified: the first are 5–8 m high, ~80 m wide and up to 1500 m long (Fig. 5F). They occur towards and along the edges of the tunnel valleys. The second type of ridge is similar in morphology but is lower in amplitude at <2 m high, 20–50 m wide and up to 600 m long, with an intra-ridge spacing of ~60 m (Fig. 5F). This type of ridge occurs further from the tunnel valley centre than the first subset of ridges. Sharp and continuous breaks in the seismic reflections beneath the ridges demonstrate that these landforms represent the top surface of retrogressive rotational slope failures within the tunnel valleys (Fig. 5C). Their morphology is nearly identical to the so-called 'glacial curvilineations' (GCLs) identified in Poland and in North America (Fig. 5D, E, 5F; Lesemann et al., 2010; Clark and

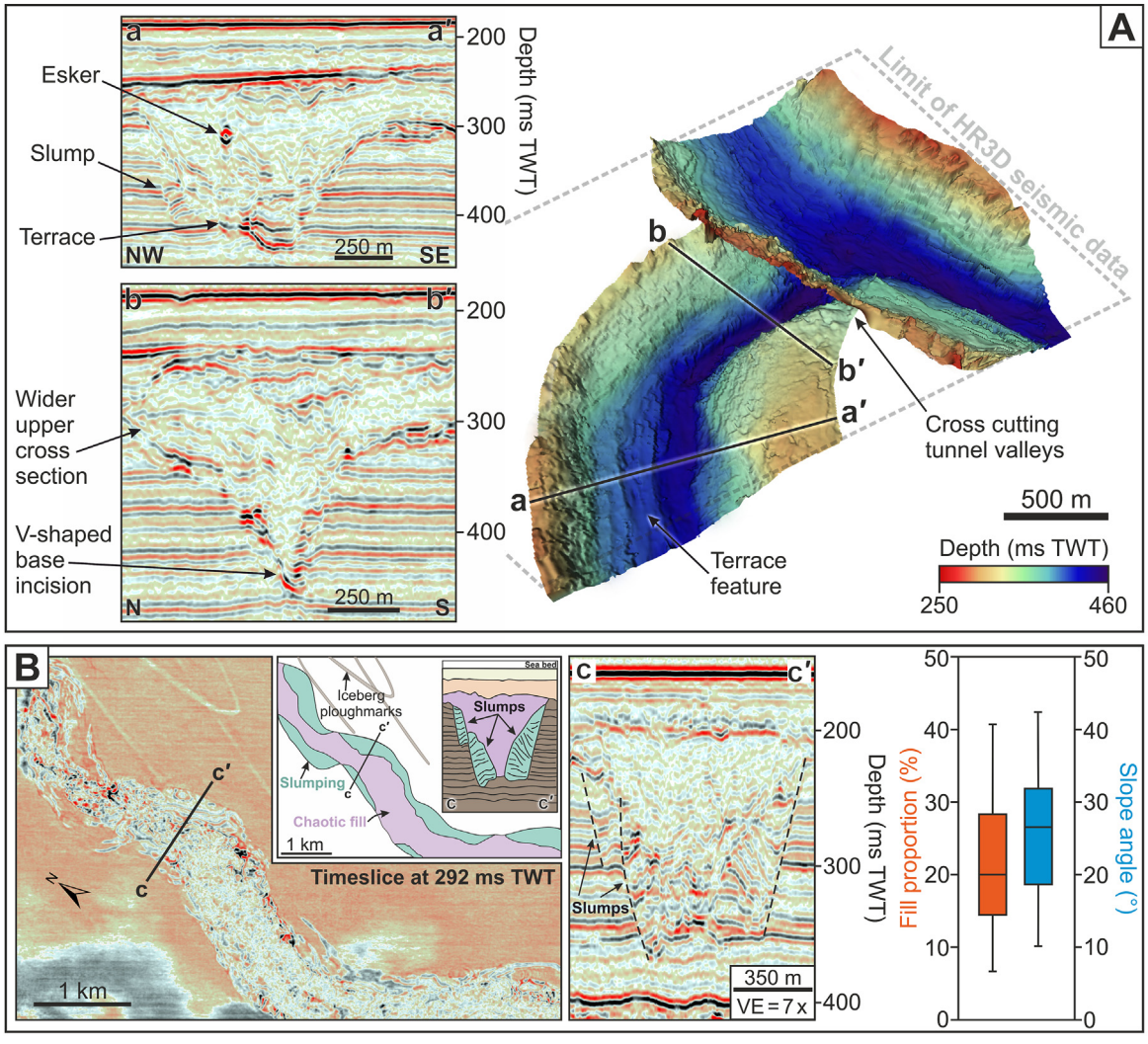

Fig. 4. Tunnel valley morphology imaged using high-resolution 3D seismic data. (A) Cross cutting tunnel valleys with a V-shaped base and broader upper cross section. The tunnel valleys contain features such as eskers within their infill, sediment slumps along their sides and sometimes contain terrace-like features like the one shown here near the base of the valley. **(B)** Examples of substantial mass movements contained within a tunnel valley. Boxplots indicate the proportion of tunnel valley infill comprised of slumped material and the slope angles of mass movements found within the tunnel valleys. Vertical exaggeration (VE) is 4 × in (A) and 7 × in (B). TWT — two-way travel time.

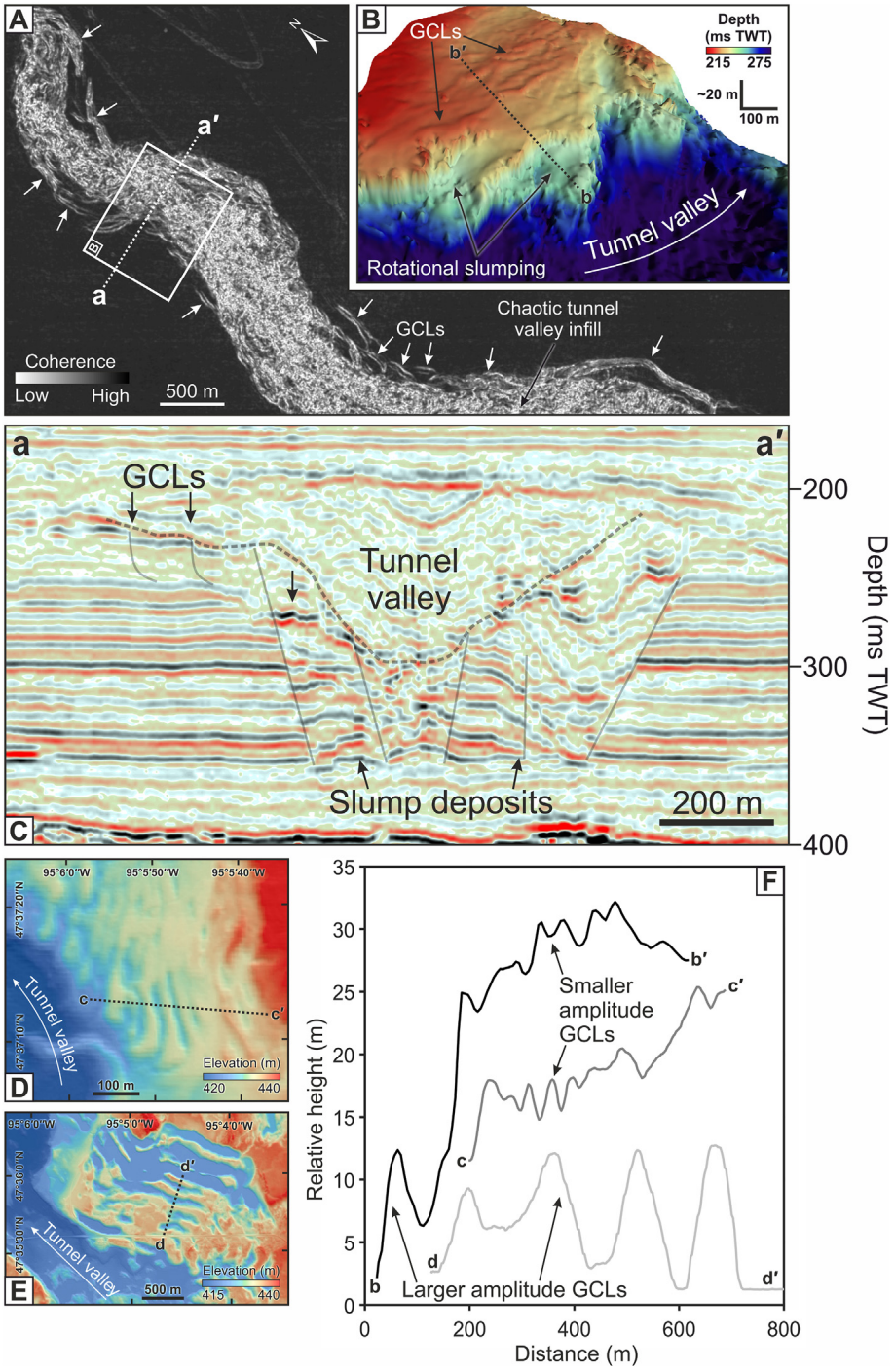

Fig. 5. Buried glacial curvilineations (GCLs) imaged within tunnel valleys. (A) Timeslice of seismic coherence at 290 ms TWT displaying curvilinear seismic anomalies (GCLs) along the sides of a tunnel valley in high-resolution 3D seismic data. **(B)** Oblique view of a picked seismic surface displaying GCLs and rotational slump scars along the tunnel valley sides. **(C)** Seismic section displaying the location of GCLs, slump deposits and faulting (semi-transparent lines) within the tunnel valley. **(D, E)** Examples of terrestrial GCLs in North America identified by Clark and Livingstone (2018) using the USA's national elevation dataset (NED) (http://nationalmap.gov/elevation.html). **(F)** Profiles of relative height across the GCLs present within the tunnel valley compared to terrestrial examples in North America.

Livingstone, 2018; Adamczyk et al., 2022), leading us to propose that these are the first subsurface examples of these features to be identified.

The tunnel valleys identified in the HR3D seismic data are characterised by undulating thalwegs (Fig. 6A) and sometimes contain smaller channels, both individual and organised in networks, incised into their bases (Fig. 6A, B, 6C). When organised in networks, these smaller channels diverge around bar-like features that are 55–540 m long and 30–165 m wide; the bars are typically narrower than the channels which intersect them. Most of the smaller channels present within the tunnel valleys are 80 m wide and ~6 m deep on average, although some attain widths of up to 250 m and depths of 15 m; they are typically ~5–10 times narrower and 3–15 times shallower than the tunnel valleys in which they are

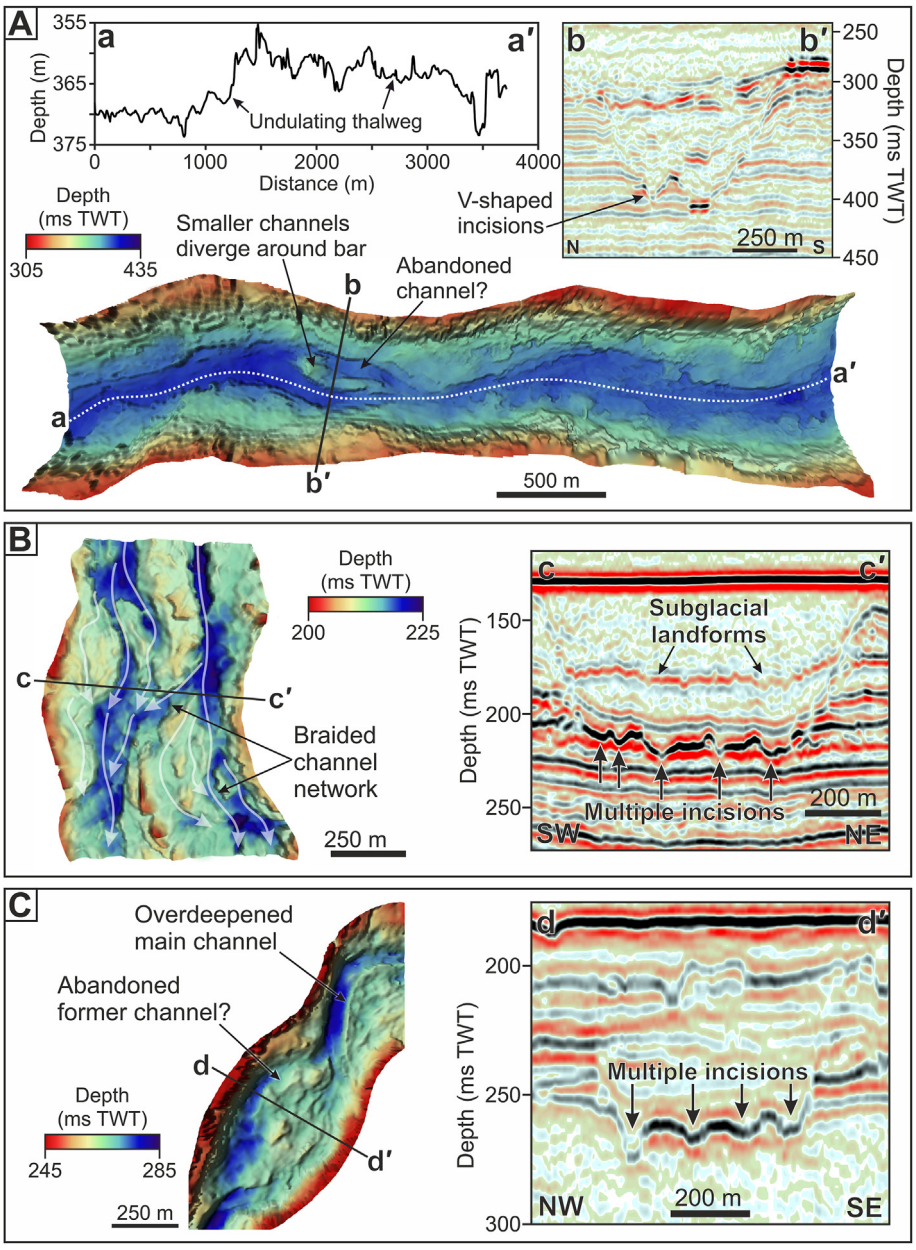

Fig. 6. Smaller channel systems comprising the base of some tunnel valleys. (A) Base of a tunnel valley displaying smaller channelised V-shaped incisions which diverge around a bar-like feature where a previous channel has been abandoned. The channel thalweg undulates. **(B)** System of braided channels incised into the base of a tunnel valley. The tunnel valley also contains subglacial landforms buried midway within its infill (see Fig. 3C in Kirkham et al., 2021). **(C)** Overdeepened channel system at the base of a tunnel valley demonstrating abandonment of a previous channel.

located. These smaller channels are relatively straight with sinuosity indexes <1.4, and sometimes appear to have been abandoned in favour of a more recently incised channel (Fig. 6A and C). Under ice-surface slopes typical of the margins of contemporary and palaeo ice sheets, these smaller channels present at the base of some valleys could carry discharges of up to 18,000 $m^3\ s^{-1}$ if filled to the bankfull level. In contrast, the entire tunnel valley structures, being several orders of magnitude larger in cross-sectional area, could potentially carry discharges of 0.5–2 $\times$ 10^7 $m^3\ s^{-1}$ if filled to their bankfull capacity.

At the resolution of the HR3D seismic data, the tunnel valleys do not contain any evidence for streamlined ice flow, such as glacial lineations, at their bases or within their infill. However, in one HR3D seismic dataset, elongate bedforms are present adjacent to a tunnel valley (Fig. 7A and B). The bedforms are <8 m high, up to 130 m wide (average = 58 m) and taper with distance away from the tunnel valley (Fig. 7B and C). They are up to 650 m long (average = 404 m) but extend beyond the boundaries of the HR3D seismic datasets in some cases, making their true length difficult to assess. The bedforms are distinct from GCLs as they are oriented oblique rather than parallel to the tunnel valley sides, are less sinuous in form, and taper with distance away from the tunnel valley. Their tapered morphology and elongation ratios of 5–10:1 are similar to other streamlined subglacial bedforms such as crag-and-tails or drumlins (Ely et al., 2016; Fransner et al., 2016), indicating that they are the imprint of fast-flowing ice over the substrate (Stokes and Clark, 2002). The continuation of the seismic reflection corresponding to the streamlined bedforms within the

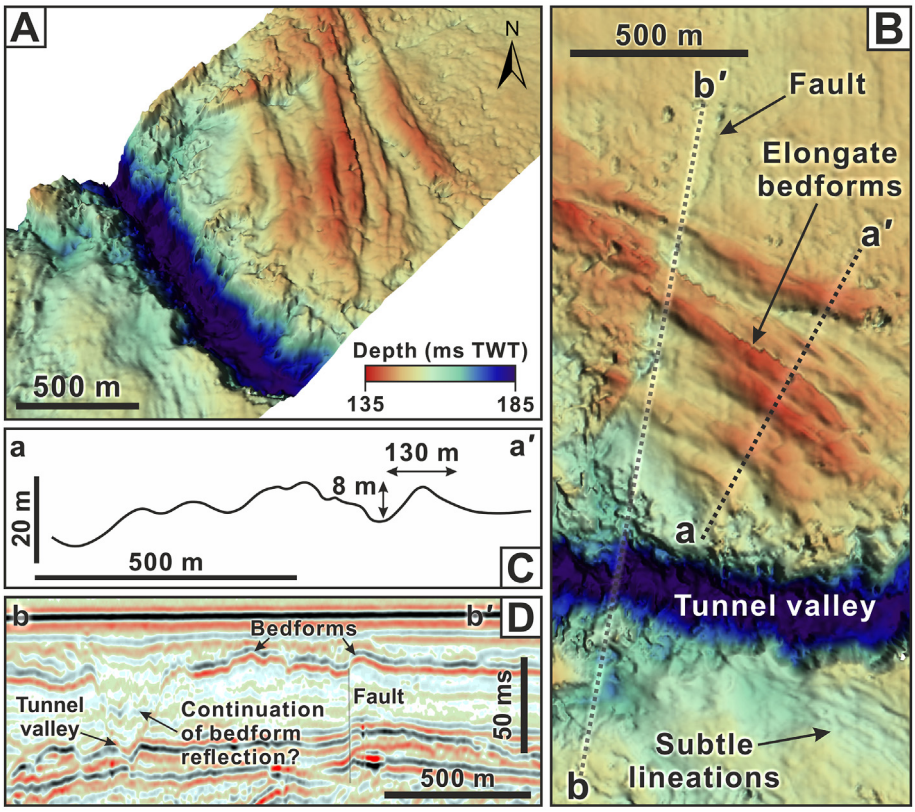

Fig. 7. Elongate bedforms present adjacent to a tunnel valley. (**A**) Oblique and (**B**) plan view of the tunnel valley and onset of the bedforms. (**C**) Depth-converted profile across the bedforms displaying a series of undulations corresponding to each ridge. (**D**) Seismic section across the tunnel valley and bedforms — note the continuation of the bedform reflection midway within the tunnel valley infill.

tunnel valley possibly suggests that they formed at a time when the tunnel valley was operating (Fig. 7D).

3.2. Modelled water routing

Fig. 8 shows the steady-state subglacial water discharges for the British-Irish and Fennoscandian ice sheets as they grow, coalesce, and the retreat across the North Sea between 27 ka and 18 ka. A large proportion of the ice-sheet bed is predicted to be at the pressure melting point, except at the 21 ka full-glacial time when the majority of the bed beneath the ice sheet in its interior is frozen (white areas). Basal melt rates are, unsurprisingly, predicted to be greatest along fast-flowing ice streams that drain the interior of the ice sheets, attaining rates of 10–60 mm yr^{-1}; these rates are similar to basal melt rates predicted beneath Antarctic ice streams during the Last Glacial Maximum (Golledge et al., 2012, 2013).

The relatively smooth inferred topography of the central North Sea Plateau provides few opportunities for water to pool, although some water ponding does occur in the Norwegian Channel and in some locations around the terrestrial margins of the UK (Fig. 8). Instead, hydraulic potential gradients force water towards the ice-sheet margins, forming long dendritic to linear channel networks which flow away from the main ice sheet accumulation centres. Large basal topographic features, such as the Norwegian Channel, also act to steer subglacial water flow. The main pathways of water routing remain relatively consistent throughout deglaciation (Fig. 8).

The ice-sheet configuration at 27 ka, during ice-sheet build-up, is characterised by low subglacial water discharges of <0.01 m^3 s^{-1} in its interior where water is derived from basal melting alone. Some surface melting occurs around the fringes of the ice sheet, yielding steady-state subglacial discharges of 1–2 m^3 s^{-1} if the surface meltwater is assumed to propagate continuously to the bed (Fig. 8A). Similarly, little to no basal melting is predicted for the interior of the ice sheet during the Last Glacial Maximum at 21 ka, when grounded ice extends fully across the North Sea. Subglacial discharges are <1 m^3 s^{-1} around the ice sheet periphery despite the cumulative basal melt flux being routed there over long distances from the interior. However, steady-state subglacial discharges at 21 ka increase by orders of magnitude in areas where surface melting is predicted to occur, reaching 5–10 m^3 s^{-1} in some areas around the fringes of the ice sheet (Fig. 8B).

The extent and magnitude of melting increases as the ice sheet begins to deglaciate at 19 ka, resulting in subglacial discharges of 5–15 m^3 s^{-1} in areas of prominent surface melting (Fig. 8C). Substantial surface melting around the fringes of the retreating ice sheet occurs at 18 ka, generating steady-state subglacial discharges of 10–100 m^3 s^{-1} near the ice-sheet margin (Fig. 8D). Basal melt rates remain similar to other timeslices. Where present, subglacial discharges of water concentrated into channelised flow paths are generally <1 m^3 s^{-1} across the interior, whereas water is routed along the Norwegian Channel at rates of 5–10 m^3 s^{-1}. In the higher resolution case study region of northern Denmark (Fig. 9), our analysis reveals that meltwater inputs from the surface, combined with basal melt passed down from the wider catchment, forms networks of 10–70 km long channels (Fig. 9C) that are semi-regularly spaced ~1–12 km apart (Fig. 9D).

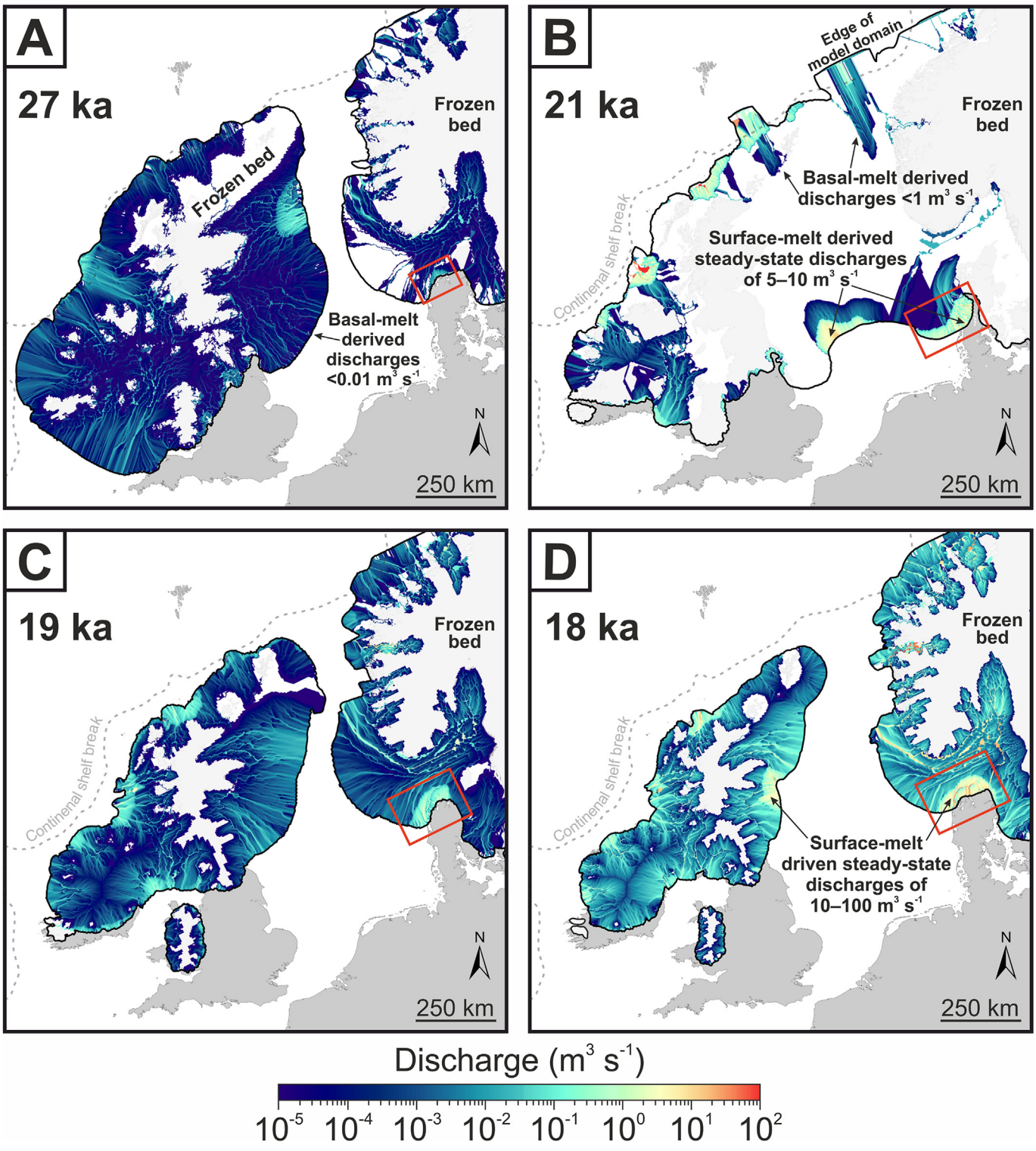

Fig. 8. Modelled water flow paths and fluxes beneath the British-Irish and Fennoscandian ice sheets. Subglacial water routing and discharge beneath grounded ice calculated at a 1500-m grid resolution at **(A)** 27 ka, **(B)** 21 ka, **(C)** 19 ka, and **(D)** 18 ka before present day timeslices. Areas of cold-based ice are displayed in white. Stippled grey line indicates the continental shelf break. Inset red boxes display the location of the high-resolution (50-m) model runs conducted across the northern Denmark for each timeslice. (For interpretation of the references to colour in this figure legend, the reader is referred to the Web version of this article.)

3.3. Tunnel valley erosion

3.3.1. Erosion from seasonal surface drainage

Erosion rate experiments were run over the regions of northern Denmark shown in Figs. 8 and 9A where the high-resolution modelling (50-m grid) of subglacial water flow was conducted. In the seasonal surface drainage scenario, we assume that all melt-water propagates to the bed of the ice sheet over a 4-month drainage season where it is routed through networks of 100-m wide channels similar to those observed in the HR3D seismic

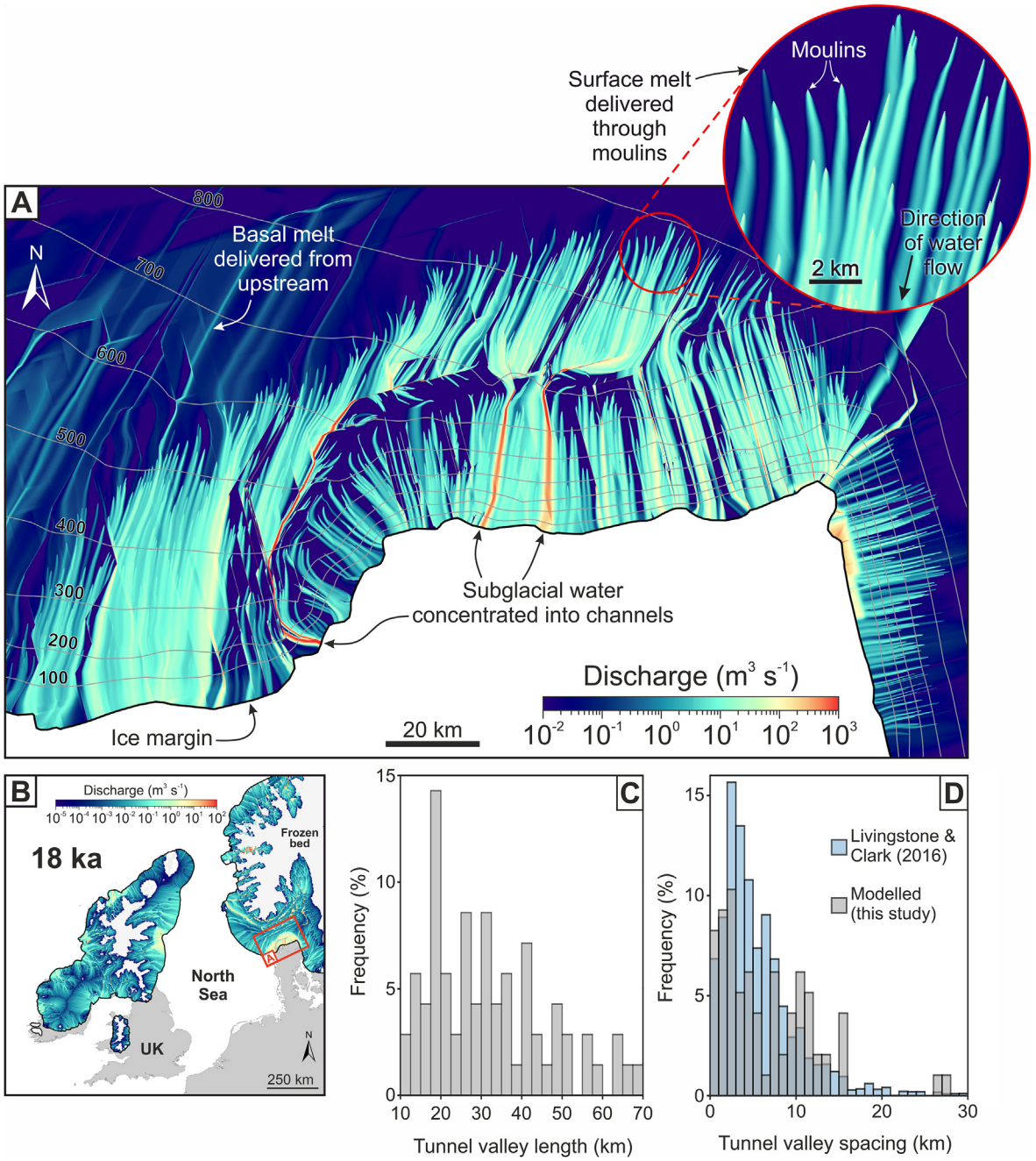

Fig. 9. Example of a detailed subglacial water routing model run and resulting tunnel valley properties. (**A**) A 50-m resolution subglacial water routing model run across northern Denmark at 18 ka, displaying the distribution of surface meltwater delivered to the ice-sheet bed through synthetic 'moulins' (inset) and the resulting subglacial channels predicted by the model. Contour lines display ice thickness. Panel B displays the location of (A) in the context of the broader water routing modelling run at a 1500-m resolution; note the change in scale bar limits from the main panel. (**C**) Distribution of the lengths of the simulated tunnel valleys in the high-resolution 50-m model runs between 18 ka–27 ka. (**D**) Distribution of tunnel valley spacing simulated in the high-resolution 50-m model runs between 18 ka–27 ka compared to those of terrestrial tunnel valleys in North America from Livingstone and Clark (2016).

data (Fig. 6). This results in average input discharges per moulin of 1–4 $m^3\ s^{-1}$ at 27 ka, 5–10 $m^3\ s^{-1}$ at 21 ka and 10–20 $m^3\ s^{-1}$ at 18 ka and 19 ka. Water discharges are greatest near the ice-sheet margin as the inputs from multiple moulins coalesce, resulting in average channel discharges of <20 $m^3\ s^{-1}$ for the 27 ka model run, 50–300 $m^3\ s^{-1}$ at 21 ka, and 50–900 $m^3\ s^{-1}$ for 18 ka and 19 ka timeslices.

When routed through 100-m wide channels, erosion generally exceeds deposition within the channels for the 18 ka, 19 ka, and 21 ka model runs. However, deposition dominates at 27 ka, especially for coarser (D_{15} = 0.1 mm) grain-size distributions due to the relatively low water discharges at this timeslice (Fig. 10A). It is possible to achieve a small amount of erosion with finer grain size distributions (D_{15} = 0.01 mm) within 10 km of the ice-sheet terminus (Fig. 10E); however, erosion rates remain extremely low (up to 1.2×10^{-6} m d^{-1}) and deposition dominates further up-ice. Thus, little subglacial meltwater erosion is possible at 27 ka.

Channel erosion dominates in the 21 ka simulations. The median erosion rate within the channels increases by up to two orders of magnitude from the start of a channel to positions near the ice-

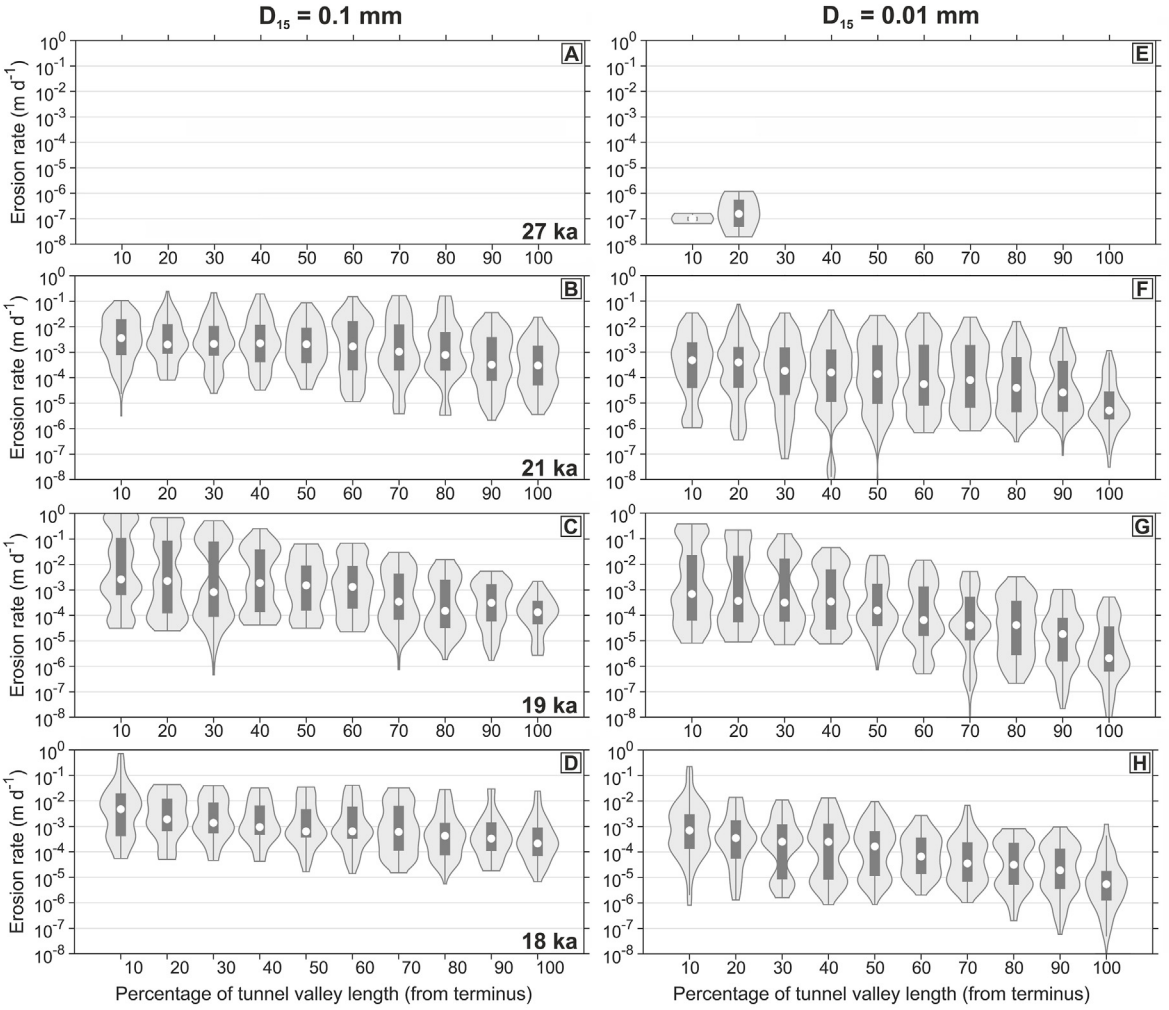

Fig. 10. Tunnel valley erosion rates into a sedimentary substrate as a proportion of modelled tunnel valley length for the seasonal drainage mechanism (migrating 100 m wide channels). Results are shown for the different model timeslices between 18 ka and 27 ka and D_{15} grain sizes of 0.1 mm and 0.01 mm (A–D and E–H).

sheet terminus. The last 50% of the tunnel valley length near the ice-sheet terminus is the most erosive; this corresponds to lengths of ~25–35 km from the ice-sheet margin. Median erosion rates near the ice-sheet terminus are ~0.003 m d^{-1}, with a 75th percentile value of ~0.02 m d^{-1}, and maximum erosion rates of 0.22 m d^{-1} are calculated for D_{15} grain sizes of 0.1 mm. Reducing the D_{15} grain size parameter to 0.01 mm (medium–fine silts) lowers erosion rates by approximately an order of magnitude (Fig. 10B and F). The highest erosion rates are calculated for the 18 ka and 19 ka timeslice model runs. For D_{15} grain sizes of 0.1 mm (very fine sands), median erosion rates near the terminus are ~0.005 m d^{-1}, with a 75th percentile value of ~0.05 m d^{-1}, although erosion rates of up to 0.7 m d^{-1} are calculated for some channels (Fig. 10C, D, 10G, 10H).

The erosion rates we calculate (Fig. 10) would be capable of incising shallow channels into a sedimentary substrate over the course of one melt season during deglaciation. For example, the 75th percentile erosion rate of 0.05 m d^{-1} at 18 ka and 19 ka would erode a channel ~6 m deep and 100 m wide in a single ablation season. Thus, it would take ~300 years to carve a valley with similar dimensions (1 km wide, 180 m deep) to those observed in northern Denmark or the North Sea if this smaller channel migrated laterally each melt season. Typical median incision rates (0.003–0.005 m d^{-1}) would result in valley formation within ~5000 years. It is therefore possible to incise large meltwater channels within tens of kilometres of the ice-sheet margin from seasonal surface melt alone over time periods of just hundreds to a few thousands of years.

3.3.2. *Erosion from outburst floods*

When routed down a 500-m wide flood channel, the 10-day drainage of a 4 km^3 lake results in total downward erosion of ~0.5–4 m into a sedimentary substrate depending on the grain-size distribution chosen. Scaling this up to the 15 km^3 lake drainage scenario, a 500-m wide channel would be eroded downwards by several tens of metres over the 10-day period. However, the erosive impact of these flooding events reduces substantially when the channel width is increased to 1000 m owing to a significant reduction in average water velocity across the channel cross section. In this latter (1000-m wide channel) scenario, total erosion reaches up to ~0.1 m for the 4 km^3 lake drainage, and up to 4 m of downward erosion is achieved for the 15 km^3 lake drainage scenario.

Our calculated basal melt rates are up to 10–60 mm yr^{-1} during the last glacial period, resulting in basal water fluxes that are generally below 0.5 m^3 s^{-1} (Fig. 8). At these values, minimum lake refilling times are ~250 years for a 4 km^3 lake and ~950 years for a 15-km^3 lake if the lakes were refilled by basal melting alone. Assuming that the lakes drain when filled to full capacity, it would

therefore take ~6000 years to carve a 500-m wide, 100-m deep tunnel valley from a 4 km^3 lake, or ~4000 years for a 15 km^3 lake. Wider valleys (>1000 m) would take considerably longer to form.

4. Discussion

4.1. Morphological insights into tunnel valley incision processes

Examination of detailed tunnel valley morphology in the HR3D seismic data yields the following observations: (i) the basal portion of tunnel valley cross sections are often several times narrower and more V-shaped compared to the upper cross sections, which are typically more U-shaped (see profile b–b′ in Fig. 4A); (ii) steep slump deposits are often buried inside the tunnel valleys and, when present, comprise ~10–40% of their infill; (iii) subglacial landforms formed by grounded ice are often buried within the middle of the tunnel valley infill (Kirkham et al., 2021); (iv) networks of smaller channels are sometimes resolvable at the base of the tunnel valleys, typically ~5–10 times narrower and 3–15 times shallower than the larger tunnel valley tracts in which they are situated. Many of these features cannot be resolved using conventional 3D seismic-reflection methods, so the processes they represent may have previously been overlooked in models of tunnel valley genesis (Kirkham et al., 2021).

The composite V/U shaped channel cross-sectional morphology is a commonly observed feature of tunnel valleys incised into unconsolidated sediments and subglacial meltwater channels incised into bedrock (e.g., Hepp et al., 2012; Kirkham et al., 2019; Larter et al., 2019; Kirkham et al., 2020; Lohrberg et al., 2020; Hogan et al., 2022) and likely reflects widening of the upper channel cross section by ice which deformed downwards into the top of the channel. The movement of deforming basal ice through the upper parts of the tunnel valley, or the eventual removal of ice from the valley, may have acted to destabilise the valley sides and trigger the mass movements now contained within the tunnel valleys, enlarging their lateral extent through glacial erosion. This morphology suggests that grounded ice likely persisted within the tunnel valleys as they were incised and filled, and is supported by the deposition of subglacial landforms such as eskers and crevasse squeeze ridges within their infill (Kirkham et al., 2021). Many of these landforms are buried at depths of more than 100 m from the tunnel valley top; based on this, we infer that as much as 65–75% of the tunnel valley cross section was filled with and sculpted by grounded ice. We suggest, therefore, that ice-contact erosion plays an important role in excavating and widening tunnel valleys in unconsolidated sediments.

We do not resolve any deformation structures along the base and sides of the channels which would suggest that sediment creep into low pressure channels is responsible for the formation of the tunnel valleys (Fig. 1C; Shoemaker, 1986; Boulton and Hindmarsh, 1987; Mooers, 1989) although we accept that these features may be unresolvable even in our HR3D seismic data. A similar lack of evidence for extensively deformed sediment adjacent to tunnel valleys has been reported from terrestrial outcrops (Ó Cofaigh, 1996; Jørgensen and Sandersen, 2006; Kehew et al., 2012). By contrast, the composite V/U-shaped profile of many tunnel valley cross sections (Hepp et al., 2012; Lohrberg et al., 2020, Fig. 4A), combined with the presence of slump deposits and subglacial landforms buried midway inside the tunnel valley fills (Kirkham et al., 2021), indicate that basal ice likely deformed extensively into the valleys. This process would be conducive to maintaining consistently high water pressures as the tunnel valleys were incised, even after relatively large channel dimensions were attained. The persistent pressurisation of the water at the base of the tunnel valleys by overlying ice, combined with the unconsolidated nature of the sediments into which tunnel valleys are usually incised, may explain how these features attain such characteristically large depths (up to ~500 m deep) (e.g., Praeg, 2003; Montelli et al., 2020). Relatively high basal water pressures within the tunnel valleys also concur with observations gathered from terrestrial outcrops of sediment injections into the preglacial substrates underlying tunnel valleys (e.g., Ghienne et al., 2007; van der Vegt et al., 2012; Ravier et al., 2014).

Relatively high basal water pressures within the tunnel valleys are also supported by the presence of smaller channel networks located at the base of the features (Fig. 6). It is not clear whether the smaller channel networks observed inside some tunnel valleys indicate that the tunnel valleys experienced pulses of high water discharges released from dammed lakes or from the ice-sheet surface (Lewington et al., 2020; Bellwald et al., 2021) or may simply reflect the expected mechanism for subglacial water flow over unconsolidated thick sedimentary beds (Walder and Fowler, 1994), such as those comprising the North Sea Basin (Lamb et al., 2018; Ottesen et al., 2018, 2020). Similar braided channel structures have been replicated in laboratory experiments simulating pressurised water flow over an erodible non-cohesive bed (Catania and Paola, 2001). However, the abandonment of smaller channels in favour of others within some tunnel valleys (Fig. 6A and C) may suggest that the smaller channel networks reflect lateral switching between different channels. This abandonment and wandering behaviour has been observed in laboratory experiments of tunnel valley formation (Lelandais et al., 2016), and may be analogous, albeit on a smaller scale, to the 'cut-and-fill' structures reported inside some terrestrial tunnel valleys (Jørgensen and Sandersen, 2006). These observations are consistent with the gradual incision of a much larger tunnel valley tract through focussed, yet relatively small, fluxes of water rather than incision by catastrophic floods.

4.1.1. The origin of glacial curvilineations

Glacial curvilineations (GCLs) were first identified in Poland (Nechay, 1927) and were later genetically associated with tunnel valleys based on their typical parallelism to the valley sides (Lesemann et al., 2010). Two competing theories have been suggested to explain the origin of GCLs in relation to tunnel valley formation. The first suggests that GCLs represent the erosional remnants of longitudinal vortices in water flow that developed during catastrophic outburst floods that produced the tunnel valleys (Lesemann et al., 2010, 2014). However, abrupt changes in observed GCL direction which mimic the tunnel valley edge are difficult to reconcile with this hypothesis as the vortices would become disrupted with such sudden changes in flow routing direction (Clark and Livingstone, 2018). This observation led Clark and Livingstone (2018) to propose an alternative hypothesis in which GCLs form through incremental mass movements at the sides of the tunnel valleys. In this hypothesis, GCLs reflect the widening of the tunnel valley sides through slope failures. However, this hypothesis was proposed solely on the basis of morphological properties, and the authors note that further structural and sedimentological information is required to determine the origin of GCLs.

Our HR3D seismic data allow the formation of GCLs to be definitively linked to slope failure processes along the sides of tunnel valleys (Fig. 5C). The largest GCLs observed within the tunnel valleys are associated with bulbous headwall scarps as described in other locations (Fig. 5B; Clark and Livingstone, 2018). Sharp breaks in seismic reflections beneath these ridges demonstrate that they formed through retrogressive rotational slope failures, propagating from the centre of the tunnel valley toward its sides, resulting in localised valley widening. The smaller ridges

reflect a continuation of the same process, but with less disruption to the underlying sediments, as the slope failures began to stabilise with increasing distance from the tunnel valley centre. The Polish and North American examples of GCLs occur within tunnel valleys that are not entirely infilled, making it difficult to untangle the timing of their formation relative to tunnel valley incision and infilling. Our HR3D seismic data demonstrate that the formation of the GCLs occurred prior to tunnel valley infilling, linking slope destabilisation and failure to tunnel valley downcutting. The formation of GCLs through slope failure of the underlying strata is also consistent with the variable internal composition of these features on land (Lesemann et al., 2014), implying that their composition will change according to the underlying substrate type rather than reflecting their formative process. Our data therefore strongly support the association between GCL genesis and slope failures triggered in response to tunnel valley incision, rather than the alternative interpretation in which broad sheet-like floods are invoked to explain their formation.

4.2. Mechanisms and rates of tunnel valley erosion

Our results demonstrate that the contribution of basal melt to the subglacial hydrological system is generally small, often 3–5 orders of magnitude smaller than the contribution from surface melting in the ablation zone. Accordingly, steady-state water fluxes derived from basal melting alone are too low (typically <1 $m^3\ s^{-1}$) to facilitate tunnel valley erosion. This finding is consistent with ideas about meltwater channel erosion beneath past ice sheets elsewhere (e.g., Lowe and Anderson, 2003; Nitsche et al., 2013; Dowdeswell et al., 2016; Kirkham et al., 2019). The dimensions of the smaller channel networks within the tunnel valleys constrain the likely discharges responsible for valley incision. At 80 m wide and ~6 m deep on average, the smaller channels could carry a maximum discharge of ~18,000 $m^3\ s^{-1}$ if filled to the bankfull level beneath a steep ice-sheet margin. Channels of these dimensions would be capable of accommodating small outburst floods from trapped lakes, such as the 4 km^3 lake drainage scenario (peak discharge of ~20,000 $m^3\ s^{-1}$). Alternatively, these smaller channel networks might reflect the cumulative erosive imprint of seasonal surface meltwater drainage. The conservative seasonal erosion rates predicted by our model demonstrate that it would be possible to erode 100-m wide channels that are several metres deep in one ablation season. Therefore, the smaller channels sometimes observed at the base of tunnel valleys may also reflect a single ablation season's erosion.

In contrast, the tunnel valleys, being several orders of magnitude larger in cross-sectional area, could hold maximum discharges of $0.5 - 2\times 10^7\ m^3\ s^{-1}$ if filled to the bankfull stage. Floods of this size would be amongst the largest ever reported on Earth (O'Connor and Costa, 2004). We consider it highly unlikely that the extensive networks of tunnel valleys observed in the North Sea, and elsewhere, were eroded by such huge discharges given the absence of large water reservoirs in any of our model predictions (Fig. 8), and the fact that our geophysical observations suggest that the tunnel valleys were largely filled by ice as they were incised. Based on these arguments, we rule out the formation of entire tunnel valleys (kilometres wide, hundreds of metres deep) from single mega outburst flooding events in this region.

Our modelling results demonstrate that both the seasonal input of surface meltwater and outburst flooding from smaller trapped lakes are viable mechanisms of incising large channels into thick sequences of unconsolidated soft sediments on timescales of hundreds to thousands of years. However, whilst seasonal surface drainage can produce networks of semi-regularly spaced tunnel valleys, the outburst flooding mechanism is only capable of forming one channel in association with a specific lake. We note that the spacing distribution for the channels predicted in the high-resolution seasonal water routing model runs is similar to other inventories of terrestrial tunnel valleys (Fig. 9D) (Livingstone and Clark, 2016). Such spacings are not reproduced when lake drainage is invoked. We therefore suggest that whilst both processes may operate during the deglaciation of ice sheets, the dominant mechanism responsible for tunnel valley formation is the drainage of surface meltwater to the bed with relatively small water fluxes.

The inference that outburst flooding assumes a relatively minor role in forming tunnel valleys during deglaciation is supported by the low number of terrestrial tunnel valleys which terminate in outwash fans in North America (Livingstone and Clark, 2016). The presence of large boulders (>2 m diameter) comprising proglacial fans at the termination of some tunnel valleys is often taken as evidence for formation in catastrophic outbursts, because the transportation of such large clasts would require discharges of at least several hundred $m^3\ s^{-1}$ (Cutler et al., 2002). However, systematic mapping of tunnel valleys across the southern sector of the former Laurentide Ice Sheet by Livingstone and Clark (2016) revealed that only a small percentage of tunnel valleys in this region (~10%) actually terminated in outwash fans. This observation is consistent with the scarcity of lakes predicted during the last deglaciation across the North Sea (Fig. 8), in particular because relatively large volumes of water (>4 km^3) are required to form just a single tunnel valley within the timescales implied by Sandersen et al. (2009). Furthermore, the regular spacing of many tunnel valley networks implies that multiple valleys were operating simultaneously across a broad spatial area as they were incised. This observation is difficult to reconcile with episodic outbursts of water released from independent reservoirs (Livingstone and Clark, 2016). Thus, although outburst flooding may play a role in the formation of some tunnel valleys (e.g., Piotrowski, 1994; Cutler et al., 2002; Livingstone and Clark, 2016; Zoet et al., 2019), this mechanism does not appear to be a pre-requisite for their formation.

In contrast, our modelling results demonstrate that, when focussed in relatively narrow channels operating within larger valley tracts, the input of surface meltwater to the subglacial hydrological system during deglaciation is capable of incising large tunnel valleys within hundreds to thousands of years (Fig. 11). Our erosion modelling supports previous interpretations of tunnel valleys being formed within tens of kilometres of the margins of receding ice sheets in the presence of steep ice-surface slopes (Kristensen et al., 2008; van der Vegt et al., 2012; Livingstone and Clark, 2016), as our predicted erosion rates are highest within the 20–30 km region upstream of the ice-sheet terminus (Fig. 10). These relatively steep ice-surface slopes would produce steep hydraulic potential gradients and drive subglacial water towards the ice-sheet margin with high water velocities; this may permit relatively low water discharges to rapidly erode sediment (Beaud et al., 2016, 2018). Accounting for ice margin retreat rates of 50–100 m yr^{-1} across northern Denmark, this zone of maximum subglacial meltwater erosion would have had 200–600 years to erode the tunnel valleys before grounded ice retreated from the area. Our erosion rates from seasonal meltwater inputs are therefore capable of incising large tunnel valleys within the timescales constrained by Sandersen et al. (2009), particularly if glacial erosion (by ice) of the upper tunnel valley cross section also contributed to valley widening.

In addition to the input of surface meltwater through perennially open moulins and crevasses, subglacial meltwater erosion rates may have been temporarily elevated by the sudden release of water trapped in supraglacial lakes through rapid drainage events. When

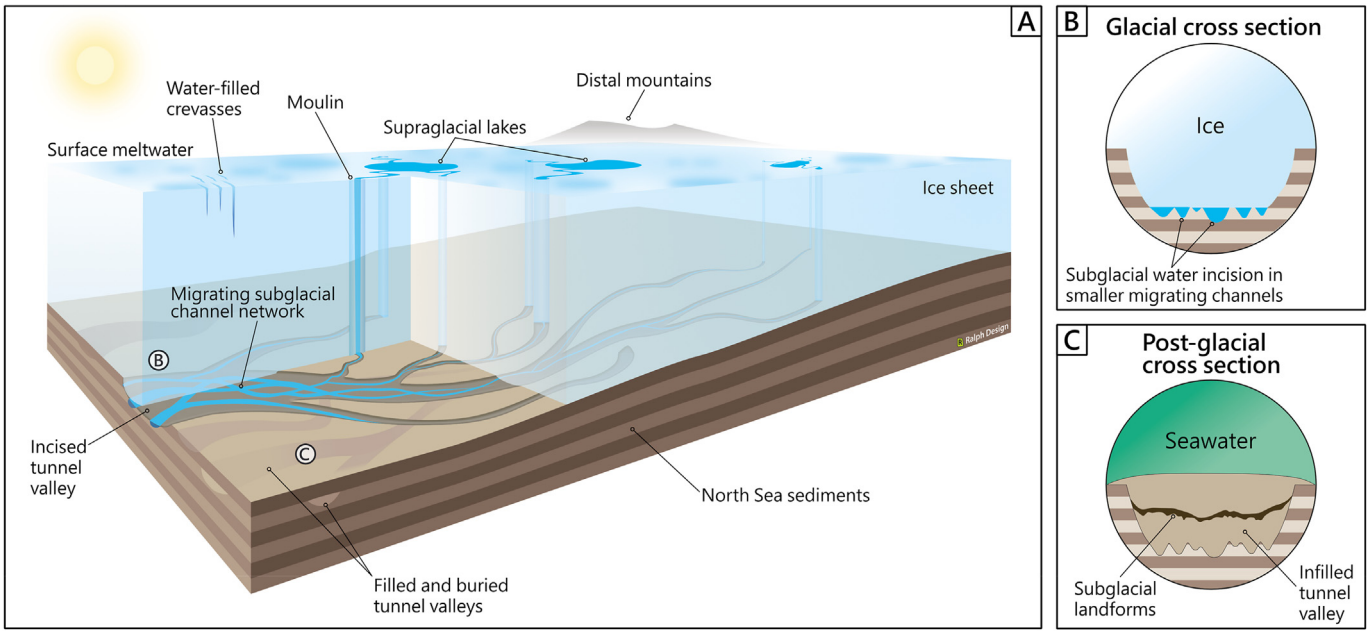

Fig. 11. Tunnel valley formation beneath a deglaciating mid-latitude ice sheet. (**A**) Idealised cutaway schematic demonstrating tunnel valley incision through the action of a network of migrating subglacial channels fed by the regular seasonal input of supraglacial meltwater into the subglacial hydrological system. (**B**) Idealised cross section of a tunnel valley being incised by smaller migrating subglacial channels during a glacial period. (**C**) Idealised cross section of a buried tunnel valley (now submerged) in a post-glacial configuration. The tunnel valley is infilled and contains subglacial landforms within it.

hydrographs from rapid Greenland supraglacial lake drainage events (e.g., Das et al., 2008; Chudley et al., 2019) are used to force our erosion model, these short-lived (hours to days) water influxes could rapidly erode decimetres to metres of sediment if focussed within a pre-existing 100–500 m wide channel. These events may therefore help to elevate erosion rates within the tunnel valleys. However, these must be taken as maximum rates as models of the input of supraglacial lake water into the subglacial hydrological system have demonstrated that these large floods tend to form a several kilometre wide turbulent blister beneath the ice sheet (Dow et al., 2015), which would reduce water velocities compared to a situation in which the water was directly concentrated into a channel.

Despite elevated erosion rates caused by supraglacial lake drainage, we do not consider this as a dominant mechanism of tunnel valley formation. This is because rapid supraglacial lake drainage events observed on present-day ice sheets only transport a small fraction of the total meltwater available from the ice-sheet surface (Koziol et al., 2017). For example, a Greenland-wide survey of supraglacial lakes between 2005 and 2009 demonstrated that only ~13% of lakes drained rapidly (Selmes et al., 2011), with the remainder draining through overtopping into meltwater streams which route water into moulins (Smith et al., 2015). Supraglacial meltwater streams are also capable of transporting far larger volumes of water into the subglacial system than even the largest supraglacial lake drainage events. For example, after the 2012 melt event which briefly thawed 97% of the surface of the Greenland Ice Sheet, the total volume of water transported in supraglacial river networks in a region of south west Greenland over a 5-day period (0.19 ± 0.05 km^3; Smith et al. (2015)) was many times greater than the volume of water delivered to the ice-sheet bed during large supraglacial lake drainage events (0.044 km^3 for Das et al., 2008).

Similar, albeit probably more extreme, conditions are likely experienced during ice-sheet deglaciation, providing a mechanism by which tunnel valleys are incised by an abundance of supraglacial meltwater released and transported to the bed by the wastage of the ice sheet. This mechanism is supported by the tendency for tunnel valleys to increase in density towards recessional ice-sheet margins (Mooers, 1989). As the timescales associated with surface melting on glaciers varies from days to hundreds of years, it is likely that the input of surface meltwater to the subglacial hydrological system regularly fluctuated with events such as the addition of surface meltwater from supraglacial lake overtopping (Tedesco et al., 2013; Smith et al., 2015), supraglacial lake drainage via hydrofracture (Das et al., 2008; Chudley et al., 2019), or intense rainfall events (e.g., Doyle et al., 2015). Such pulses of water would have resulted in enhanced erosion as high discharges entered the basal hydrological system (Huuse and Lykke-Andersen, 2000). Furthermore, the conversion of gravitational potential energy to heat in the basal drainage system as surface meltwater drains to the ice-sheet bed can increase basal melt rates by up to two orders of magnitude during periods of intense surface melting or rainfall events (Young et al., 2022). Although this process is not included in the model setup used here, this mechanism would increase the erosive potential of surface meltwater drainage events for tunnel valley incision; therefore, the tunnel valley incision rates reported here are likely conservative.

The burial of subglacial landforms at significant depths (>100 m) within the tunnel valleys examined here (Figs. 4A and 6B; Kirkham et al., 2021) demonstrates extensive deformation of ice into the tunnel valleys. This deformation would likely have caused a surface expression in the overlying ice sheet. Basal channels observed beneath Antarctic ice shelves have surface expressions in the form of localised ice lowering along their lengths which can divert surface meltwater into supraglacial rivers and contribute to hydrofracturing (Dow et al., 2018). A similar feedback mechanism might be expected in the case of tunnel valleys; as ice deforms into the incising tunnel valley, greater amounts of water are focussed into surficial troughs expressed on the ice-sheet surface — contributing to hydrofracturing and supplying additional meltwater that can be used to further incise the tunnel valley. This feedback mechanism might help to explain the great depths that

tunnel valleys are capable of incising during relatively short periods of time.

Our results demonstrate that it is possible for tunnel valleys to be incised over hundreds to thousands of years by the action of smaller channels fed by the regular seasonal input of supraglacial meltwater into the subglacial hydrological system (Fig. 11). Combined with ice widening of the upper channel cross section, this process could erode extensive networks of tunnel valleys, mostly filled with ice as they were incised (Nordmann, 1958; Smed, 1962; Krüger, 1989; Smed, 1998; Huuse and Lykke-Andersen, 2000).

4.3. Implications for tunnel valley genesis and ice-sheet dynamics

The long-standing debate regarding the genesis of tunnel valleys has focussed on the viability of catastrophic versus steady-state formation hypotheses. Our results confirm that both of these mechanisms are possible, and may lead to similar valley forms. Some authors have previously made a distinction between tunnel valleys and tunnel channels, whereby tunnel channels are genetically associated with bankfull flooding conditions, a single ice margin, lack tributaries and have consistent dimensions along their length, whereas tunnel valleys may have more complex morphologies and infill (Clayton et al., 1999; Kehew et al., 2012). Our geophysical observations and numerical modelling results support this genetic difference, and potentially provide additional criteria with which these different landforms can be distinguished. Our HR3D seismic data reveal that tunnel valleys may have smaller channels buried inside them and often contain evidence of glaciotectonism and extensive ice widening within the upper section of the valleys (Figs. 4 and 6; Kirkham et al., 2021). In contrast, tunnel channels are likely to be smaller, straighter, and associated with an individual accumulation of subglacial water (Clayton et al., 1999; Kehew and Kozlowski, 2007; Kehew et al., 2012). For example, tunnel channels formed by subglacial lake drainage in the Green Bay Lobe, Wisconsin, are 450 m wide and 65 m deep (Zoet et al., 2019). They are considerably smaller than other tunnel valleys formed from surface meltwater during the same glacial period elsewhere (e.g., kilometres wide and 100s m deep; Sandersen et al. (2009)).

Accordingly, tunnel channel formation can be viewed as an isolated process that occurs under specific circumstances, such as that in which basal topography permits large scale impounding of water. In contrast, the injection of large volumes of surface meltwater to the ice-sheet bed over a broad area is capable of rapidly generating regularly spaced networks of tunnel valleys if surface melt rates are high enough. This mechanism likely explains the majority of tunnel valley formation in formerly glaciated regions of soft-sediment substrates such as the North Sea. Whilst tunnel valleys buried in the North Sea are notoriously difficult to date, they can be separated into multiple generations by their crosscutting patterns (Lonergan et al., 2006; Kristensen et al., 2007; Stewart and Lonergan, 2011; Stewart et al., 2013; Ottesen et al., 2020). Our results demonstrate that it would be possible to erode each of these tunnel valley generations within a single glacial-deglacial cycle — and possibly multiple tunnel valley generations if ice readvances occurred in the presence of significant meltwater availability. It may therefore be reasonable to associate each generation of tunnel valleys with a particular glaciation, and from this reconstruct ice-sheet extents and the hydrological conditions experienced during each deglaciation based on the distribution and form of that generation of tunnel valleys (Stewart and Lonergan, 2011; Stewart et al., 2013; Ottesen et al., 2020; Kirkham et al., 2021). However, in principle, it is also possible that multiple generations of tunnel valleys could be incised by a dynamic ice sheet within a single glaciation given the rapid incision rates indicated by our numerical modelling results.

Our analysis supports a growing body of work which suggests that subglacial meltwater is an extremely powerful geomorphic agent, capable of carving large channels into unconsolidated substrates over hundreds to thousands of years (Sandersen et al., 2009; Beaud et al., 2016, 2018). The rapid formation of large subglacial valleys over potentially just hundreds of years has implications for ice-sheet dynamics. Previous laboratory experiments have suggested that tunnel valley formation may act to stabilise portions of ice sheets undergoing deglaciation through the rapid evacuation of basal water, potentially preventing catastrophic ice-sheet collapse (Lelandais et al., 2018). Similar conclusions have been drawn from the palaeo-record in some locations (Patterson, 1997). Our numerical modelling results indicate that stable evacuation of such water is possible within timescales of hundreds of years — rapid when viewed in the context of deglacial timescales. However, contrasting assemblages of subglacial landforms imaged inside and around some tunnel valleys imply that the formation of these channels may be associated with both stable and dynamic ice behaviour (Fig. 6; Kirkham et al., 2021). Thus, further work, including numerical modelling of the overlying ice response, is needed to elucidate the impact that tunnel valley formation has on the dynamics of deglaciating ice sheets. This could inform on a potentially key process that may regulate the stability of deglaciating ice sheets in the future (e.g., Hulbe, 2017).

5. Conclusions

We performed a series of numerical experiments informed by new observations from high-resolution 3D seismic analysis that explore the rates and mechanisms at which tunnel valleys are formed beneath deglaciating mid-latitude ice sheets. These new seismic observations reveal a number of morphological clues as to the mechanisms of tunnel valley formation that are not resolvable using conventional 3D seismic-reflection methods. Smaller abandoned channel systems and braided channel networks present at the base of larger tunnel valley tracts indicate that these features are carved through the action of migrating smaller channels. In addition, extensive slump deposits and subglacial landforms buried within the tunnel valleys demonstrate that pervasive ice contact erosion was a key process regulating their morphology and dimensions.

Our numerical modelling of subglacial water flux and sediment erosion demonstrate that migrating narrow channels fed by seasonal surface meltwater are capable of incising networks of tunnel valleys 1–2 km wide and hundreds of metres deep over just hundreds to thousands of years during deglaciation — timescales that are commensurate with independent geological evidence of rapid tunnel valley formation in this region. Modelled erosion rates reach maximum values within tens of kilometres of the ice-sheet terminus, implying that tunnel valleys form time-transgressively close to the margins of retreating ice sheets. This mechanism likely accounts for the formation of most regularly spaced tunnel valley networks found in formerly glaciated regions. Outburst floods from topographically confined basins can also lead to large-scale channel incision over thousands of years; however, this process is only likely to apply in specific circumstances, some of which may now be decipherable using advances in HR3D seismic data. Further incorporation of palaeo-subglacial hydrological evidence into ice-sheet models will help to elucidate the role that tunnel valley formation may have on the dynamics of past and contemporary ice sheets during deglaciation.

Author contributions

J.D.K., K.A.H., R.D.L., J.A.D., and N.S.A. conceived the study. E.S., K.G. and M.H. worked with data owners to gain permission for the use of the 3D seismic data in this project. J.D.K. analysed the 3D seismic data with contributions from K.A.H., R.D.L., J.A.D., E.S., M.H., M.A.S., and D.O. The BRITICE-CHRONO model data were provided by J.C.E. and C.D.C. The water routing and erosion modelling experiments were conducted by J.D.K. with contributions from N.S.A and J.C.E. J.D.K. wrote the initial draft of the manuscript and produced the figures. All authors contributed to data interpretation and writing of the final paper.

Declaration of competing interest

The authors declare that they have no known competing financial interests or personal relationships that could have appeared to influence the work reported in this paper.

Data availability

The authors do not have permission to share data.

Acknowledgements

We thank bp, Harbour Energy, Equinor Energy AS, Lundin Energy Norway AS, Petoro AS, Aker BP ASA, TotalEnergies EP Norge AS for access and permission to publish images extracted from the HR3D seismic data. S&P Global and Schlumberger are thanked for providing academic seismic interpretation software licenses. James D. Kirkham is supported by the Natural Environment Research Council (grant NE/L002507/1). Kelly A. Hogan and Robert D. Larter were supported by the Natural Environment Research Council – British Antarctic Survey Polar Science for Planet Earth programme. Jeremy C. Ely acknowledges support from a Natural Environmental Research Council independent fellowship (NE/R014574/1). Chris Clark is supported by the European Research Council (ERC) under the European Union's Horizon 2020 research and innovation programme (Grant agreement No. 787263; PalGlac). We thank Calvin Shackleton and an anonymous reviewer for helpful reviews that improved the paper. The interpretations made in this paper are the views of the authors and not necessarily those of the license owners.

References

Adamczyk, A., Wysota, W., Piotrowski, J.A., 2022. Inventory of glacial curvilineations (GCLs) at the southern periphery of the last Scandinavian Ice Sheet. Geomorphology 400, 108094. https://doi.org/10.1016/j.geomorph.2021.108094.

Andrews, L.C., Catania, G.A., Hoffman, M.J., Gulley, J.D., Lüthi, M.P., Ryser, C., Hawley, R.L., Neumann, T.A., 2014. Direct observations of evolving subglacial drainage beneath the Greenland Ice Sheet. Nature 514 (7520), 80–83. https://doi.org/10.1038/nature13796.

Arnold, N., 2010. A new approach for dealing with depressions in digital elevation models when calculating flow accumulation values. Prog. Phys. Geogr.: Earth Environ. 34 (6), 781–809. https://doi.org/10.1177/0309133310384542.

Atkinson, N., Andriashek, L.D., Slattery, S.R., 2013. Morphological analysis and evolution of buried tunnel valleys in northeast Alberta, Canada. Quat. Sci. Rev. 65, 53–72. https://doi.org/10.1016/j.quascirev.2012.11.031.

Banwell, A.F., Willis, I.C., Arnold, N.S., 2013. Modeling subglacial water routing at Paakitsoq, W Greenland. J. Geophys. Res.: Earth Surf. 118 (3), 1282–1295. https://doi.org/10.1002/jgrf.20093.

Banwell, A., Hewitt, I., Willis, I., Arnold, N., 2016. Moulin density controls drainage development beneath the Greenland ice sheet. J. Geophys. Res.: Earth Surf. 121 (12), 2248–2269. https://doi.org/10.1002/2015jf003801.

Bartholomew, I., Nienow, P., Sole, A., Mair, D., Cowton, T., Palmer, S., Wadham, J., 2011. Supraglacial forcing of subglacial drainage in the ablation zone of the Greenland ice sheet. Geophys. Res. Lett. 38 (8), L08502. https://doi.org/10.1029/2011gl047063.

Batchelor, C.L., Margold, M., Krapp, M., Murton, D.K., Dalton, A.S., Gibbard, P.L., Stokes, C.R., Murton, J.B., Manica, A., 2019. The configuration of Northern Hemisphere ice sheets through the Quaternary. Nat. Commun. 10 (1), 3713. https://doi.org/10.1038/s41467-019-11601-2.

Beaud, F., Flowers, G.E., Venditti, J.G., 2016. Efficacy of bedrock erosion by subglacial water flow. Earth Surf. Dyn. 4 (1), 125–145. https://doi.org/10.5194/esurf-4-125-2016.

Beaud, F., Venditti, J.G., Flowers, G.E., Koppes, M., 2018. Excavation of subglacial bedrock channels by seasonal meltwater flow. Earth Surf. Process. Landforms 43 (9), 1960–1972. https://doi.org/10.1002/esp.4367.

Bell, R.E., Banwell, A.F., Trusel, L.D., Kingslake, J., 2018. Antarctic surface hydrology and impacts on ice-sheet mass balance. Nat. Clim. Change 8 (12), 1044–1052. https://doi.org/10.1038/s41558-018-0326-3.

Bellwald, B., Planke, S., Polteau, S., Lebedeva-Ivanova, N., Faleide, J.I., Morris, S.M., Morse, S., Castelltort, S., 2021. Characterization of a glacial paleo-outburst flood using high-resolution 3-D seismic data: bjørnelva River Valley, SW Barents Sea. J. Glaciol. 1–17. https://doi.org/10.1017/jog.2020.115.

Benvenuti, A., Šegvić, B., Moscariello, A., 2018. Tunnel valley deposits from the southern North Sea - material provenance and depositional processes. Boreas 47 (2), 625–642. https://doi.org/10.1111/bor.12292.

Björnsson, H., 1992. Jokulhlaups in Iceland: prediction, characteristics and simulation. Ann. Glaciol. 16, 95–106. https://doi.org/10.3189/1992AoG16-1-95-106.

Björnsson, H., 2002. Subglacial lakes and jokulhlaups in. Iceland: Global Planet. Change 35, 255–271. https://doi.org/10.1016/S0921-8181(02)00130-3.

Boulton, G.S., Hindmarsh, R.C.A., 1987. Sediment deformation beneath glaciers: rheology and geological consequences. J. Geophys. Res. 92. https://doi.org/10.1029/JB092iB09p09059. B9.

Bradley, S.L., Ely, J.C., Clark, C.D., Edwards, R., Shennan, I., Hindmarsh, R.C.A., 2018. Glacial isostatic adjustment of the British Isles and north west Europe. EGU General Assembly Conference Abstracts 20, 9701. https://ui.adsabs.harvard.edu/abs/2018EGUGA..20.9701B.

Brennand, T.A., Shaw, J., 1994. Tunnel channels and associated landforms south central Ontario their implications for ice sheet hydrology. Can. J. Earth Sci. 31 (3), 505–522. https://doi.org/10.1139/e94-045.

Carter, S.P., Fricker, H.A., Siegfried, M.R., 2017. Antarctic subglacial lakes drain through sediment-floored canals: theory and model testing on real and idealized domains. Cryosphere 11 (1), 381–405. https://doi.org/10.5194/tc-11-381-2017.

Catania, G., Paola, C., 2001. Braiding under glass: Geol. 29 (3), 259–262. https://doi.org/10.1130/0091-7613(2001)029<0259:BUG>2.0.CO;2, 2.

Chudley, T.R., Christoffersen, P., Doyle, S.H., Bougamont, M., Schoonman, C.M., Hubbard, B., James, M.R., 2019. Supraglacial lake drainage at a fast-flowing Greenlandic outlet glacier. Proc. Natl. Acad. Sci. U. S. A. 116 (51), 25468–25477. https://doi.org/10.1073/pnas.1913685116.

Clark, C.D., Livingstone, S.J., 2018. Glacial curvilineations found along the southern sector of the Laurentide Ice sheet and a hypothesis of formation involving subglacial slope failure in tunnel valleys and subglacial lakes. Earth Surf. Process. Landforms 43 (7), 1518–1528. https://doi.org/10.1002/esp.4324.

Clark, C. D., Ely, J. C., Hindmarsh, R. C. A., Bradley, S. L., Igneczi, A., Fabel, D., Ó Cofaigh, C., Chiverrell, R. C., Scourse, J. D., Benetti, S., Bradwell, T., Evans, D. J. A., Roberts, D. H., Burke, M. J., Callard, S. L., Medialdea, A., Saher, M. H., Small, D., Smedley, R. K., Gasson, E., Gregoire, L., Gandy, N., Ballantyne, C., Bateman, M. D., Bigg, G. R., Doole, J., Dove, D., Duller, G. A. T., C., H. A. L., Jenkins, G. T. H., Livingstone, S. J., McCarron, S., Moreton, S. G., Pollard, D., Praeg, D., Sejrup, H. P., Van Landeghem, K., and Wilson, P., In review, Growth and retreat of the last British-Irish Ice Sheet, 31,000 to 15,000 years ago: the BRITICE-CHRONO reconstruction: Boreas.

Clark, C.D., Ely, J.C., Greenwood, S.L., Hughes, A.L.C., Meehan, R., Barr, I.D., Bateman, M.D., Bradwell, T., Doole, J., Evans, D.J.A., Jordan, C.J., Monteys, X., Pellicer, X.M., Sheehy, M., 2018. BRITICE Glacial Map, version 2: a map and GIS database of glacial landforms of the last British-Irish Ice Sheet. Boreas 47 (1), 11–27. https://doi.org/10.1111/bor.12273.

Clark, C.D., Chiverrell, R.C., Fabel, D., Hindmarsh, R.C.A., Ó Cofaigh, C., Scourse, J.D., 2021. Timing, pace and controls on ice sheet retreat: an introduction to the BRITICE-CHRONO transect reconstructions of the British–Irish Ice Sheet. J. Quat. Sci. 36 (5), 673–680. https://doi.org/10.1002/jqs.3326.

Clayton, L., Attig, J.W., Mickelson, D.M., 1999. Tunnel channels formed in Wisconsin during the last glaciations. In: Mickelson, D.M., Attig, J.W. (Eds.), Glacial Processes Past and Present: USA, vol. 337. Geological Society of Amercia Special Paper, pp. 69–82.

Colgan, W., Steffen, K., 2009. Modelling the spatial distribution of moulins near Jakobshavn, Greenland. IOP Conf. Ser. Earth Environ. Sci. 6, 1. https://doi.org/10.1088/1755-1307/6/1/012022.

Cuffey, K.M., Paterson, W.S.B., 2010. The Physics of Glaciers. Academic Press.

Cutler, P.M., Colgan, P.M., Mickelson, D.M., 2002. Sedimentologic evidence for outburst floods from the Laurentide Ice Sheet margin in Wisconsin, USA: implications for tunnel channel formation. Quat. Int. 90, 23–40. https://doi.org/10.1016/S1040-6182(01)00090-8.

Damsgaard, A., Suckale, J., Piotrowski, J.A., Houssais, M., Siegfried, M.R., Fricker, H.A., 2017. Sediment behavior controls equilibrium width of subglacial channels. J. Glaciol. 63 (242), 1034–1048. https://doi.org/10.1017/jog.2017.71.

Das, S.B., Joughin, I., Behn, M.D., Howat, I.M., King, M.A., Lizarralde, D., Bhatia, M.P., 2008. Fracture propagation to the base of the Greenland Ice Sheet during supraglacial lake drainage. Science 320 (5877), 778–781. https://doi.org/10.1126/science.1153360.

Douillet, G., Ghienne, J.F., Géraud, Y., Abueladas, A., Diraison, M., Al-Zoubi, A., 2012.

Late Ordovician tunnel valleys in southern Jordan. Geol. Soc. Lond. Special Pub. 368 (1), 275–292. https://doi.org/10.1144/sp368.4.
Dow, C.F., Kulessa, B., Rutt, I.C., Tsai, V.C., Pimentel, S., Doyle, S.H., van As, D., Lindback, K., Pettersson, R., Jones, G.A., Hubbard, A., 2015. Modeling of subglacial hydrological development following rapid supraglacial lake drainage. J Geophys Res Earth Surf 120 (6), 1127–1147. https://doi.org/10.1002/2014JF003333.
Dow, C.F., Lee, W.S., Greenbaum, J.S., Greene, C.A., Blankenship, D.D., Poinar, K., Forrest, A.L., Young, D.A., Zappa, C.J., 2018. Basal channels drive active surface hydrology and transverse ice shelf fracture. Sci. Adv. 4 (6), eaao7212. https://doi.org/10.1126/sciadv.aao7212.
Dowdeswell, J.A., Canals, M., Jakobsson, M., Todd, B.J., Dowdeswell, E.K., Hogan, K.A., 2016. The variety and distribution of submarine glacial landforms and implications for ice-sheet reconstruction. In: Dowdeswell, J.A., Canals, M., Jakobsson, M., Todd, B.J., Dowdeswell, E.K., Hogan, K.A. (Eds.), Atlas of Submarine Glacial Landforms: Modern, Quaternary and Ancient: London. Geological Society, London, Memoirs, pp. 519–552.
Doyle, S.H., Hubbard, A., van de Wal, R.S.W., Box, J.E., van As, D., Scharrer, K., Meierbachtol, T.W., Smeets, P.C.J.P., Harper, J.T., Johansson, E., Mottram, R.H., Mikkelsen, A.B., Wilhelms, F., Patton, H., Christoffersen, P., Hubbard, B., 2015. Amplified melt and flow of the Greenland ice sheet driven by late-summer cyclonic rainfall. Nat. Geosci. 8 (8), 647–653. https://doi.org/10.1038/ngeo2482.
Ely, J.C., Clark, C.D., Spagnolo, M., Stokes, C.R., Greenwood, S.L., Hughes, A.L.C., Dunlop, P., Hess, D., 2016. Do subglacial bedforms comprise a size and shape continuum? Geomorphology 257, 108–119. https://doi.org/10.1016/j.geomorph.2016.01.001.
EMODnet Bathymetry Consortium, 2018. In: Consortium, E.B. (Ed.), EMODnet Digital Bathymetry (DTM 2018). https://doi.org/10.12770/18ff0d48-b203-4a65-94a9-5fd8b0ec35f6.
Fransner, O., Noormets, R., Flink, A.E., Hogan, K.A., 2016. Crag-and-tail landforms in outer rijpfjorden, nordaustlandet, svalbard. In: Dowdeswell, J.A., Canals, M., Jakobsson, M., Todd, B.J., Dowdeswell, E.K., Hogan, K.A. (Eds.), Atlas of Submarine Glacial Landforms: Modern, Quaternary and Ancient, ume 46. The Geological Society of London, pp. 57–58.
Games, K.P., 2012. Shallow gas detection - why HRS, why 3D, why not HRS 3D? First Break 30, 25–33. https://doi.org/10.3997/1365-2397.2012016.
Gandy, N., Gregoire, L.J., Ely, J.C., Cornford, S.L., Clark, C.D., Hodgson, D.M., 2019. Exploring the ingredients required to successfully model the placement, generation, and evolution of ice streams in the British-Irish Ice Sheet. Quat. Sci. Rev. 223. https://doi.org/10.1016/j.quascirev.2019.105915.
Ghienne, J.F., Deynoux, M., 1998. Large scale channel fill structures in Late Ordovician glacial deposits in Mauritania, Western Sahara. Sediment. Geol. 119 (1–2), 141–159. https://doi.org/10.1016/S0037-0738(98)00045-1.
Ghienne, J.F., Le Heron, D.P., Moreau, J., Denis, M., Deynoux, M., 2007. The Late Ordovician glacial sedimentary system of the North Gondwana platform. In: Hambrey, M.J., Christoffersen, P., Glasser, N.F., Hubbard, B. (Eds.), Glacial Sedimentary Processes and Products. Wiley, pp. 295–319.
Giglio, C., Benetti, S., Sacchetti, F., Lockhart, E., Hughes Clarke, J., Plets, R., Van Landeghem, K., Ó Cofaigh, C., Scourse, J., Dunlop, P., 2021. A Late Pleistocene channelized subglacial meltwater system on the Atlantic continental shelf south of Ireland. Boreas 51, 118–135. https://doi.org/10.1111/bor.12536.
Gledhill, L.A., Williamson, A.G., 2017. Inland advance of supraglacial lakes in northwest Greenland under recent climatic warming. Ann. Glaciol. 59 (76pt1), 66–82. https://doi.org/10.1017/aog.2017.31.
Golledge, N.R., Fogwill, C.J., Mackintosh, A.N., Buckley, K.M., 2012. Dynamics of the last glacial maximum Antarctic ice-sheet and its response to ocean forcing. Proceedings National Acad. Sci. United States Am. 109 (40), 16052–16056. https://doi.org/10.1073/pnas.1205385109.
Golledge, N.R., Levy, R.H., McKay, R.M., Fogwill, C.J., White, D.A., Graham, A.G.C., Smith, J.A., Hillenbrand, C.-D., Licht, K.J., Denton, G.H., Ackert, R.P., Maas, S.M., Hall, B.L., 2013. Glaciology and geological signature of the Last Glacial Maximum Antarctic Ice Sheet. Quat. Sci. Rev. 78, 225–247. https://doi.org/10.1016/j.quascirev.2013.08.011.
Gowan, E.J., Zhang, X., Khosravi, S., Rovere, A., Stocchi, P., Hughes, A.L.C., Gyllencreutz, R., Mangerud, J., Svendsen, J.-I., Lohmann, G., 2021. A new global ice sheet reconstruction for the past 80 000 years. Nat. Commun. 12 (1), 1199. https://doi.org/10.1038/s41467-021-21469-w.
Gudmundsson, M.T., Björnsson, H., Pálsson, F., 1995. Changes in jökulhlaup sizes in Grímsvötn, Vatnajökull, Iceland, 1934-91, deduced from in-situ measurements of subglacial lake volume. J. Glaciol. 41 (138), 263–272. https://doi.org/10.3189/S0022143000016166.
Hepp, D.A., Hebbeln, D., Kreiter, S., Keil, H., Bathmann, C., Ehlers, J., Mörz, T., 2012. An east-west-trending Quaternary tunnel valley in the south-eastern North Sea and its seismic-sedimentological interpretation. J. Quat. Sci. 27 (8), 844–853. https://doi.org/10.1002/jqs.2599.
Hirst, J.P.P., Benbakir, A., Payne, D.F., Westlake, I.R., 2002. Tunnel valleys and density flow processes in the upper Ordovician glacial succession, Illizi Basin, Algeria: influence on reservoir quality. J. Petrol. Geol. 25 (3), 297–324. https://doi.org/10.1111/j.1747-5457.2002.tb00011.x.
Hogan, K.A., Arnold, N.S., Larter, R.D., Kirkham, J.D., Noormets, R., Ó Cofaigh, C., Golledge, N.R., Dowdeswell, J.A., 2022. Subglacial water flow over an antarctic palaeo-ice stream bed. J. Geophys. Res.: Earth Surf. 127, 2. https://doi.org/10.1029/2021jf006442.
Hooke, R.L., Jennings, C.E., 2006. On the formation of the tunnel valleys of the southern Laurentide ice sheet. Quat. Sci. Rev. 25 (11–12), 1364–1372. https://doi.org/10.1016/j.quascirev.2006.01.018.
Hulbe, C., 2017. Is ice sheet collapse in West Antarctica unstoppable? Science 356 (6341), 910–911. https://doi.org/10.1126/science.aam9728.
Huuse, M., Lykke-Andersen, H., 2000. Overdeepened Quaternary valleys in the eastern Danish North Sea morphology and origin. Quat. Sci. Rev. 19, 1233–1253. https://doi.org/10.1016/S0277-3791(99)00103-1.
Iverson, N., Hooyer, T.S., Baker, R.W., 1998. Ring-shear studies of till deformation: coulomb-plastic behaviour and distributed strain in glacier beds. J. Glaciol. 44 (148), 634–642. https://doi.org/10.3189/S0022143000002136.
Iverson, N., Hooyer, T.S., Fischer, U.H., Cohen, D., Moore, P.L., Jackson, M., Lappegard, G., Kohler, J., 2007. Soft-bed experiments beneath Engabreen, Norway: regelation infiltration, basal slip and bed deformation. J. Glaciol. 53 (182), 323–340. https://doi.org/10.3189/002214307783258431.
Jentzsch, A., 1884. Über die Bildung der preussischen Seen. Zeitschrift der deutschen geologischen Gesellschaft für Erdkunde 10, 699–702.
Jordan, T.A., Ferraccioli, F., Corr, H., Graham, A., Armadillo, E., Bozzo, E., 2010. Hypothesis for Mega-Outburst Flooding from a Palaeo-Subglacial Lake beneath the East Antarctic Ice Sheet. Terra Nova, pp. 283–289. https://doi.org/10.1111/j.1365-3121.2010.00944.x.
Jørgensen, F., Sandersen, P.B.E., 2006. Buried and open tunnel valleys in Denmark—erosion beneath multiple ice sheets. Quat. Sci. Rev. 25 (11–12), 1339–1363. https://doi.org/10.1016/j.quascirev.2005.11.006.
Kehew, A.E., Kozlowski, A.L., 2007. Tunnel channels of the Saginaw lobe, Michigan, USA: applied Quaternary research in the central part of glaciated terrain. Geol. Survey Finland, Special Paper 46, 69–78.
Kehew, A.E., Piotrowski, J.A., Jørgensen, F., 2012. Tunnel valleys: concepts and controversies — a review. Earth Sci. Rev. 113 (1–2), 33–58. https://doi.org/10.1016/j.earscirev.2012.02.002.
King, E.C., 2020. The precision of radar-derived subglacial bed topography: a case study from Pine Island Glacier, Antarctica. Ann. Glaciol. 1–8. https://doi.org/10.1017/aog.2020.33.
Kingslake, J., Ely, J.C., Das, I., Bell, R.E., 2017. Widespread movement of meltwater onto and across Antarctic ice shelves. Nature 544 (7650), 349–352. https://doi.org/10.1038/nature22049.
Kirkham, J.D., Hogan, K.A., Larter, R.D., Arnold, N.S., Nitsche, F.O., Golledge, N.R., Dowdeswell, J.A., 2019. Past water flow beneath Pine Island and Thwaites Glaciers, West Antarctica. Cryosphere 13 (7), 1959–1981. https://doi.org/10.5194/tc-13-1959-2019.
Kirkham, J.D., Hogan, K.A., Larter, R.D., Arnold, N.S., Nitsche, F.O., Kuhn, G., Gohl, K., Anderson, J.B., Dowdeswell, J.A., 2020. Morphometry of bedrock meltwater channels on Antarctic inner continental shelves: implications for channel development and subglacial hydrology. Geomorphology 370, 107369. https://doi.org/10.1016/j.geomorph.2020.107369.
Kirkham, J.D., Hogan, K.A., Larter, R.D., Self, E., Games, K., Huuse, M., Stewart, M.A., Ottesen, D., Arnold, N.S., Dowdeswell, J.A., 2021. Tunnel valley infill and genesis revealed by high-resolution 3-D seismic data. Geol. 49 (12), 1516–1520. https://doi.org/10.1130/g49048.1.
Koziol, C.P., Arnold, N., 2018. Modelling seasonal meltwater forcing of the velocity of land-terminating margins of the Greenland Ice Sheet. Cryosphere 12 (3), 971–991. https://doi.org/10.5194/tc-12-971-2018.
Koziol, C., Arnold, N., Pope, A., Colgan, W., 2017. Quantifying supraglacial meltwater pathways in the Paakitsoq region, West Greenland. J. Glaciol. 63 (239), 464–476. https://doi.org/10.1017/jog.2017.5.
Kristensen, T.B., Huuse, M., 2012. Multistage erosion and infill of buried Pleistocene tunnel valleys and associated seismic velocity effects. Geol. Soc. Lond. Special Pub. 368 (1), 159–172. https://doi.org/10.1144/sp368.15.
Kristensen, T.B., Huuse, M., Piotrowski, J.A., Clausen, O.R., 2007. A morphometric analysis of tunnel valleys in the eastern North Sea based on 3D seismic data. J. Quat. Sci. 22 (8), 801–815. https://doi.org/10.1002/jqs.1123.
Kristensen, T.B., Piotrowski, J.A., Huuse, M., Clausen, O.R., Hamberg, L., 2008. Time-transgressive tunnel valley formation indicated by infill sediment structure, North Sea – the role of glaciohydraulic supercooling. Earth Surf. Process. Landforms 33 (4), 546–559. https://doi.org/10.1002/esp.1668.
Krüger, J., 1989. Gletscheren Og Landskabet – I Nutid Og Istid, Nordisk Forlag. Geografiske temahæfter, Copenhagen, Gyldendal.
Lamb, R.M., Harding, R., Huuse, M., Stewart, M., Brocklehurst, S.H., 2018. The early quaternary North Sea basin. J. Geol. Soc. 175 (2), 275–290. https://doi.org/10.1144/jgs2017-057.
Larter, R.D., Hogan, K.A., Hillenbrand, C.-D., Smith, J.A., Batchelor, C.L., Cartigny, M., Tate, A.J., Kirkham, J.D., Roseby, Z.A., Kuhn, G., Graham, A.G.C., Dowdeswell, J.A., 2019. Subglacial hydrological control on flow of an Antarctic Peninsula palaeo-ice stream. Cryosphere 13 (6), 1583–1596. https://doi.org/10.5194/tc-13-1583-2019.
Le Heron, D.P., Sutcliffe, O., Bourgig, K., Craig, J., Visentin, C., Whittington, R.J., 2004. Sedimentary architecture of Upper Ordovician tunnel valleys, Gargaf Arch, Libya: implications for the genesis of a hydrocarbon reservoir. GeoArabia 9 (2), 137–160.
Leeson, A.A., Shepherd, A., Briggs, K., Howat, I., Fettweis, X., Morlighem, M., Rignot, E., 2015. Supraglacial lakes on the Greenland ice sheet advance inland under warming climate. Nat. Clim. Change 5 (1), 51–55. https://doi.org/10.1038/nclimate2463.
Lelandais, T., Mourgues, R., Ravier, É., Pochat, S., Strzerzynski, P., Bourgeois, O., 2016. Experimental modeling of pressurized subglacial water flow: implications for tunnel valley formation. J. Geophys. Res.: Earth Surf. 121 (11), 2022–2041. https://doi.org/10.1002/2016jf003957.

Lelandais, T., Ravier, É., Pochat, S., Bourgeois, O., Clark, C., Mourgues, R., Strzerzynski, P., 2018. Modelled subglacial floods and tunnel valleys control the life cycle of transitory ice streams. Cryosphere 12 (8), 2759–2772. https://doi.org/10.5194/tc-12-2759-2018.

Lesemann, J.-E., Piotrowski, J.A., Wysota, W., 2010. "Glacial curvilineations": new glacial landforms produced by longitudinal vortices in subglacial meltwater flows. Geomorphology 120 (3–4), 153–161. https://doi.org/10.1016/j.geomorph.2010.03.020.

Lesemann, J.-E., Piotrowski, J.A., Wysota, W., 2014. Genesis of the 'glacial curvilineation' landscape by meltwater processes under the former Scandinavian Ice Sheet, Poland. Sediment. Geol. 312, 1–18. https://doi.org/10.1016/j.sedgeo.2014.07.003.

Lewington, E.L.M., Livingstone, S.J., Clark, C.D., Sole, A.J., Storrar, R.D., 2020. A model for interaction between conduits and surrounding hydraulically connected distributed drainage based on geomorphological evidence from Keewatin, Canada. Cryosphere 14 (9), 2949–2976. https://doi.org/10.5194/tc-14-2949-2020.

Lindbäck, K., Pettersson, R., Hubbard, A.L., Doyle, S.H., As, D., Mikkelsen, A.B., Fitzpatrick, A.A., 2015. Subglacial water drainage, storage, and piracy beneath the Greenland ice sheet. Geophys. Res. Lett. 42 (18), 7606–7614. https://doi.org/10.1002/2015gl065393.

Livingstone, S.J., Clark, C.D., 2016. Morphological properties of tunnel valleys of the southern sector of the Laurentide Ice Sheet and implications for their formation. Earth Surf. Dyn. 4 (3), 567–589. https://doi.org/10.5194/esurf-4-567-2016.

Lohrberg, A., Schwarzer, K., Unverricht, D., Omlin, A., Krastel, S., 2020. Architecture of tunnel valleys in the southeastern North Sea: new insights from high-resolution seismic imaging. J. Quat. Sci. 35, 892–906. https://doi.org/10.1002/jqs.3244.

Lonergan, L., Maidment, S.C.R., Collier, J.S., 2006. Pleistocene subglacial tunnel valleys in the central North Sea basin: 3-D morphology and evolution. J. Quat. Sci. 21 (8), 891–903. https://doi.org/10.1002/jqs.1015.

Lowe, A.L., Anderson, J.B., 2003. Evidence for abundant subglacial meltwater beneath the paleo ice sheet in Pine Island Bay, Antarctica. J. Glaciol. 49 (164), 125–138. https://doi.org/10.3189/172756503781830971.

Marshall, S.J., Tarasov, L., Clarke, G.K.C., Peltier, W.R., 2000. Glaciological reconstruction of the Laurentide Ice Sheet: physical processes and modelling challenges. Can. J. Earth Sci. 37 (5), 769–793. https://doi.org/10.1139/e99-113.

Montelli, A., Gulick, S.P.S., Fernandez, R., Frederick, B.C., Shevenell, A.E., Leventer, A., Blankenship, D.D., 2019. Seismic stratigraphy of the Sabrina Coast shelf, East Antarctica: early history of dynamic meltwater-rich glaciations. GSA Bulletin 132 (3–4), 545–561. https://doi.org/10.1130/b35100.1.

Montelli, A., Dowdeswell, J.A., Pirogova, A., Terekhina, Y., Tokarev, M., Rybin, N., Martyn, A., Khoshtariya, V., 2020. Deep and extensive meltwater system beneath the former. Eurasian Ice Sheet Kara Sea: Geol. 48, 179–183. https://doi.org/10.1130/g46968.1.

Mooers, H.D., 1989. On the formation of the tunnel valleys of the Superior Lobe Central Minnesota. Quat. Res. 32, 24–35. https://doi.org/10.1016/0033-5894(89)90029-X.

Moreau, J., Huuse, M., 2014. Infill of tunnel valleys associated with landward-flowing ice sheets: the missing Middle Pleistocene record of the NW European rivers? G-cubed 15 (1), 1–9. https://doi.org/10.1002/2013gc005007.

Mouginot, J., Rignot, E., Bjork, A.A., van den Broeke, M., Millan, R., Morlighem, M., Noel, B., Scheuchl, B., Wood, M., 2019. Forty-six years of Greenland Ice Sheet mass balance from 1972 to 2018. Proc. Natl. Acad. Sci. U. S. A. 116 (19), 9239–9244. https://doi.org/10.1073/pnas.1904242116.

Müther, D., Back, S., Reuning, L., Kukla, P., Lehmkuhl, F., 2012. Middle Pleistocene landforms in the Danish Sector of the southern North Sea imaged on 3D seismic data. In: Huuse, M., Redfern, J., Le Heron, D.P., Dixon, R.J., Moscariello, A., Craig, J. (Eds.), Glaciogenic Reservoirs and Hydrocarbon Systems, vol. 368. Geological Society, Special Publications, London, pp. 111–127.

Nechay, W., 1927. Utwory lodowcowe ziemi dobrzyńskiej. Sprawozdania Państwowego Instytutu Geologicznego 4 (1–2), 61–144.

Nienow, P.W., Sole, A.J., Slater, D.A., Cowton, T.R., 2017. Recent advances in our understanding of the role of meltwater in the Greenland ice sheet system. Curr. Clim. Change Rep. 3 (4), 330–344. https://doi.org/10.1007/s40641-017-0083-9.

Nitsche, F.O., Gohl, K., Larter, R.D., Hillenbrand, C.D., Kuhn, G., Smith, J.A., Jacobs, S., Anderson, J.B., Jakobsson, M., 2013. Paleo ice flow and subglacial meltwater dynamics in Pine Island Bay, West Antarctica. Cryosphere 7 (1), 249–262. https://doi.org/10.5194/tc-7-249-2013.

Niu, L.U., Lohmann, G., Hinck, S., Gowan, E.J., Krebs-Kanzow, U.T.A., 2019. The sensitivity of Northern Hemisphere ice sheets to atmospheric forcing during the last glacial cycle using PMIP3 models. J. Glaciol. 65 (252), 645–661. https://doi.org/10.1017/jog.2019.42.

Nordmann, V., 1958. Beskrivelse til geologisk kort over danmark. Kortbladet fredericia. A: kvartære aflejringer. Geol. Survey Denmark (Series I) 22-A, 1–125.

Ó Cofaigh, C., 1996. Tunnel valley genesis. Prog. Phys. Geogr. 20 (1), 1–19. https://doi.org/10.1177/030913339602000101.

O'Connor, J.E., Costa, J.E., 2004. The world's largest floods, past and present - their causes and magnitudes: U.S. Geol. Surv. Circular 1254, 13p.

Ottesen, D., Batchelor, C.L., Dowdeswell, J.A., Løseth, H., 2018. Morphology and pattern of quaternary sedimentation in the North Sea Basin (52–62°N). Mar. Petrol. Geol. 98, 836–859. https://doi.org/10.1016/j.marpetgeo.2018.08.022.

Ottesen, D., Stewart, M., Brönner, M., Batchelor, C.L., 2020. Tunnel valleys of the central and northern North Sea (56°N to 62°N): distribution and characteristics. Mar. Geol. 425. https://doi.org/10.1016/j.margeo.2020.106199.

Patterson, C.J., 1997. Southern Laurentide ice lobes were created by ice streams: des Moines Lobe in Minnesota. Sediment. Geol. 111, 249–261. https://doi.org/10.1016/S0037-0738(97)00018-3.

Peterson, G., Johnson, M.D., Dahlgren, S., Påsse, T., Alexanderson, H., 2018. Genesis of hummocks found in tunnel valleys: an example from Hörda. southern Sweden: GFF 140 (2), 189–201. https://doi.org/10.1080/11035897.2018.1470199.

Piotrowski, J.A., 1994. Tunnel valley formation in northwest Germany - geology mechanisms of formation and subglacial bed conditions for the Bornhoved tunnel valley. Sediment. Geol. 89, 107–141. https://doi.org/10.1016/0037-0738(94)90086-8.

Praeg, D., 1996. Morphology, stratigraphy and genesis of buried Mid-Pleistocene tunnel valleys in the southern North Sea Basin. University of Edinburgh. PhD thesis.

Praeg, D., 2003. Seismic imaging of mid-Pleistocene tunnel-valleys in the North Sea Basin—high resolution from low frequencies. J. Appl. Geophys. 53 (4), 273–298. https://doi.org/10.1016/j.jappgeo.2003.08.001.

Prins, L.T., Andresen, K.J., Clausen, O.R., Piotrowski, J.A., 2020. Formation and widening of a North Sea tunnel valley - the impact of slope processes on valley morphology. Geomorphology 368, 107347. https://doi.org/10.1016/j.geomorph.2020.107347.

Pugin, A.J.M., Oldenborger, G.A., Cummings, D.I., Russell, H.A.J., Sharpe, D.R., 2014. Architecture of buried valleys in glaciated Canadian Prairie regions based on high resolution geophysical data. Quat. Sci. Rev. 86, 13–23. https://doi.org/10.1016/j.quascirev.2013.12.007.

Ravier, E., Buoncristiani, J.-F., Guiraud, M., Menzies, J., Clerc, S., Goupy, B., Portier, E., 2014. Porewater pressure control on subglacial soft sediment remobilization and tunnel valley formation: a case study from the Alnif tunnel valley (Morocco). Sediment. Geol. 304, 71–95. https://doi.org/10.1016/j.sedgeo.2014.02.005.

Rignot, E., Mouginot, J., Scheuchl, B., van den Broeke, M., van Wessem, M.J., Morlighem, M., 2019. Four decades of antarctic ice sheet mass balance from 1979-2017. Proceedings National Acad. Sci. United States Am. 116 (4), 1095–1103. https://doi.org/10.1073/pnas.1812883116.

Sandersen, P.B.E., Jørgensen, F., Larsen, N.K., Westergaard, J.H., Auken, E., 2009. Rapid tunnel-valley formation beneath the receding Late Weichselian ice sheet in Vendsyssel, Denmark. Boreas 38 (4), 834–851. https://doi.org/10.1111/j.1502-3885.2009.00105.x.

Scambos, T.A., Hulbe, C., Fahnestock, M.A., Bohlander, J., 2000. The link between climate warming and break-up of ice shelves in the Antarctic Peninsula. J. Glaciol. 46, 516–530. https://doi.org/10.3189/172756500781833043.

Selmes, N., Murray, T., James, T.D., 2011. Fast draining lakes on the Greenland ice sheet. Geophys. Res. Lett. 38, 15. https://doi.org/10.1029/2011gl047872.

Shackleton, C., Patton, H., Hubbard, A., Winsborrow, M., Kingslake, J., Esteves, M.S.R., Andreassen, K., Greenwood, S.L., 2018. Subglacial water storage and drainage beneath the Fennoscandian and Barents Sea ice sheets. Quat. Sci. Rev. 201, 13–28. https://doi.org/10.1016/j.quascirev.2018.10.007.

Shaw, J., Gilbert, R., 1990. Evidence for large scale subglacial meltwater flood events in southern Ontario and northern New York State. Geol. 18, 1169–1172. https://doi.org/10.1130/0091-7613(1990)018<1169:EFLSSM>2.3.CO;2, 2.

Shepherd, A., Fricker, H.A., Farrell, S.L., 2018. Trends and connections across the Antarctic cryosphere. Nature 558 (7709), 223–232. https://doi.org/10.1038/s41586-018-0171-6.

Shepherd, A., Ivins, E., Rignot, E., Smith, B., van den Broeke, M., Velicogna, I., Whitehouse, P., Briggs, K., Joughin, I., Krinner, G., Nowicki, S., Payne, T., Scambos, T., Schlegel, N., Agosta, C., Ahlstrøm, A., Babonis, G., Barletta, V.R., Bjørk, A.A., Blazquez, A., Bonin, J., Colgan, W., Csatho, B., Cullather, R., Engdahl, M.E., Felikson, D., Fettweis, X., Forsberg, R., Hogg, A.E., Gallee, H., Gardner, A., Gilbert, L., Gourmelen, N., Groh, A., Gunter, B., Hanna, E., Harig, C., Helm, V., Horvath, A., Horwath, M., Khan, S., Kjeldsen, K.K., Konrad, H., Langen, P.L., Lecavalier, B., Loomis, B., Luthcke, S., McMillan, M., Melini, D., Mernild, S., Mohajerani, Y., Moore, P., Mottram, R., Mouginot, J., Moyano, G., Muir, A., Nagler, T., Nield, G., Nilsson, J., Noël, B., Otosaka, I., Pattle, M.E., Peltier, W.R., Pie, N., Rietbroek, R., Rott, H., Sandberg Sørensen, L., Sasgen, I., Save, H., Scheuchl, B., Schrama, E., Schröder, L., Seo, K.-W., Simonsen, S.B., Slater, T., Spada, G., Sutterley, T., Talpe, M., Tarasov, L., van de Berg, W.J., van der Wal, W., van Wessem, M., Vishwakarma, B.D., Wiese, D., Wilton, D., Wagner, T., Wouters, B., Wuite, J., The, I.T., 2020. Mass balance of the Greenland ice sheet from 1992 to 2018. Nature 579 (7798), 233–239. https://doi.org/10.1038/s41586-019-1855-2.

Shoemaker, E.M., 1986. Subglacial hydrology for an ice sheet resting on a deformable aquifer. J. Glaciol. 32, 20–30. https://doi.org/10.3189/S0022143000006833.

Shreve, R.L., 1972. Movement of water in glaciers. J. Glaciol. 11 (62), 205–214. https://doi.org/10.3189/S002214300002219X.

Smed, P., 1962. Studier over den fynske øgruppes glaciale landskabsformer. Med. Dan. Geol. Foren. 15, 1–74.

Smed, P., 1998. Die Entstehung der danischen und norddeutschen "Rinnentaler (tunneltäler) – glaziologische gesichtspunkte. Eiszeitalt. Ggw. 48, 1–18.

Smith, L.C., Chu, V.W., Yang, K., Gleason, C.J., Pitcher, L.H., Rennermalm, A.K., Legleiter, C.J., Behar, A.E., Overstreet, B.T., Moustafa, S.E., Tedesco, M., Forster, R.R., LeWinter, A.L., Finnegan, D.C., Sheng, Y., Balog, J., 2015. Efficient meltwater drainage through supraglacial streams and rivers on the southwest Greenland ice sheet. Proc. Natl. Acad. Sci. U. S. A. 112 (4), 1001–1006. https://doi.org/10.1073/pnas.1413024112.

Stewart, M.A., Lonergan, L., 2011. Seven glacial cycles in the middle-late Pleistocene of northwest Europe: geomorphic evidence from buried tunnel valleys. Geol. 39

(3), 283–286. https://doi.org/10.1130/g31631.1.
Stewart, M., Lonergan, L., Hampson, G., 2012. 3D seismic analysis of buried tunnel valleys in the Central North Sea: tunnel valley fill sedimentary architecture. In: Huuse, M., Redfern, J., Le Heron, D.P., Dixon, R., Moscariello, A., Craig, J. (Eds.), Glaciogenic Reservoirs and Hydrocrabon Systems, vol. 368. Geological Society, London, Special Publications, pp. 173–184.
Stewart, M.A., Lonergan, L., Hampson, G., 2013. 3D seismic analysis of buried tunnel valleys in the central North Sea: morphology, cross-cutting generations and glacial history. Quat. Sci. Rev. 72, 1–17. https://doi.org/10.1016/j.quascirev.2013.03.016.
Stokes, C.R., Clark, C.D., 2002. Are long subglacial bedforms indicative of fast ice flow? Boreas 31, 239–249. https://doi.org/10.1111/j.1502-3885.2002.tb01070.x.
Svendsen, J.I., Alexanderson, H., Astakhov, V.I., Demidov, I., Dowdeswell, J.A., Funder, S., Gataullin, V., Henriksen, M., Hjort, C., Houmark-Nielsen, M., Hubberten, H.W., Ingólfsson, Ó., Jakobsson, M., Kjær, K.H., Larsen, E., Lokrantz, H., Lunkka, J.P., Lysså, A., Mangerud, J., Matiouchkov, A., Murray, A., Möller, P., Niessen, F., Nikolskaya, O., Polyak, L., Saarnisto, M., Siegert, C., Siegert, M.J., Spielhagen, R.F., Stein, R., 2004. Late Quaternary ice sheet history of northern Eurasia. Quat. Sci. Rev. 23 (11), 1229–1271. https://doi.org/10.1016/j.quascirev.2003.12.008.
Tarasov, L., Peltier, W.R., 2004. A geophysically constrained large ensemble analysis of the deglacial history of the North American ice-sheet complex. Quat. Sci. Rev. 23 (3), 359–388. https://doi.org/10.1016/j.quascirev.2003.08.004.
Tedesco, M., 2009. Assessment and development of snowmelt retrieval algorithms over Antarctica from K-band spaceborne brightness temperature (1979–2008). Rem. Sens. Environ. 113 (5), 979–997. https://doi.org/10.1016/j.rse.2009.01.009.
Tedesco, M., Monaghan, A.J., 2009. An updated Antarctic melt record through 2009 and its linkages to high-latitude and tropical climate variability. Geophys. Res. Lett. 36 (18), L18502. https://doi.org/10.1029/2009gl039186.
Tedesco, M., Willis, I., Hoffman, M.J., Banwell, A., Alexander, P., Arnold, N., 2013. Ice dynamic response to two modes of surface lake drainage on the Greenland ice sheet. Environ. Res. Lett. 8, 034007. https://doi.org/10.1088/1748-9326/8/3/034007.
Trusel, L.D., Frey, K.E., Das, S.B., Karnauskas, K.B., Kuipers Munneke, P., van Meijgaard, E., van den Broeke, M.R., 2015. Divergent trajectories of Antarctic surface melt under two twenty-first-century climate scenarios. Nat. Geosci. 8 (12), 927–932. https://doi.org/10.1038/ngeo2563.
Tulaczyk, S., Kamb, W.B., Engelhardt, H.F., 2000a. Basal mechanics of Ice Stream B, west Antarctica: 1. Till mechanics. J. Geophys. Res. Solid Earth 105 (B1), 463–481. https://doi.org/10.1029/1999jb900329.
Tulaczyk, S., Kamb, W.B., Engelhardt, H.F., 2000b. Basal mechanics of Ice Stream B, west Antarctica: 2. Undrained plastic bed model. J. Geophys. Res. Solid Earth 105 (B1), 483–494. https://doi.org/10.1029/1999jb900328.
Ussing, N.V., 1903. Om Jyllands hedesletter og teorierne for deres dannelse. Oversigt over Det Kongelige danske Videnskabernes Selskabs Forhandlinger 2, 99–152.
Ussing, N.V., 1907. Om floddale og randmoræner i Jylland: Oversigt over Det Kongelige danske Videnskabernes Selskabs. Forhandlinger 4, 161–213.
van der Vegt, P., Janszen, A., Moscariello, A., 2012. Tunnel valleys: current knowledge and future perspectives. In: Huuse, M., Redfern, J., Le Heron, D.P., Dixon, R., Moscariello, A., Craig, J. (Eds.), Glaciogenic Reservoirs and Hydrocarbon Systems, vol. 368. Geological Society, Special Publications, London, pp. 75–97.
Walder, J.S., 1986. Hydraulics of subglacial cavities. J. Glaciol. 32 (112), 439–445. https://doi.org/10.3189/S0022143000012156.
Walder, J.S., Fowler, A.C., 1994. Channelized subglacial drainage over a deformable bed. J. Glaciol. 40 (134), 3–15. https://doi.org/10.3189/S0022143000003750.
Williams, G.P., 1989. Sediment concentration versus water discharge during single hydrologic events in rivers. J. Hydrol. 111, 89–106. https://doi.org/10.1016/0022-1694(89)90254-0.
Willis, I.C., Pope, E.L., Leysinger Vieli, G.J.M.C., Arnold, N.S., Long, S., 2016. Drainage networks, lakes and water fluxes beneath the Antarctic ice sheet. Ann. Glaciol. 57 (72), 96–108. https://doi.org/10.1017/aog.2016.15.
Wingfield, R., 1989. Glacial incisions indiciating middle and upper Pleistocene ice limits off britain. Terra. Nova 1, 538–548. https://doi.org/10.1111/j.1365-3121.1989.tb00430.x.
Wingfield, R., 1990. The origin of major incisions within the Pleistocene deposits of the North Sea. Mar. Geol. 91 (1–2), 31–52. https://doi.org/10.1016/0025-3227(90)90131-3.
Wingham, D.J., Siegert, M.J., Shepherd, A., Muir, A.S., 2006. Rapid discharge connects Antarctic subglacial lakes. Nature 440 (7087), 1033–1036. https://doi.org/10.1038/nature04660.
Winkelmann, R., Martin, M.A., Haseloff, M., Albrecht, T., Bueler, E., Khroulev, C., Levermann, A., 2011. The potsdam parallel ice sheet model (PISM-PIK) – Part 1: model description. Cryosphere 5 (3), 715–726. https://doi.org/10.5194/tc-5-715-2011.
Woodland, A.W., 1970. The buried tunnel-valleys of East Anglia. Proc. Yorks. Geol. Soc. 37, 521–578. https://doi.org/10.1144/pygs.37.4.521.
Wright, H.E., 1973. Tunnel valleys, glacial surges and subglacial hydrology of the Superior Lobe, Minnesota. In: Black, R.F., Goldthwait, R.P., Willman, H.B. (Eds.), The Wisconsinan Stage. Geological Society of America, pp. 251–276.
Young, T.J., Christoffersen, P., Bougamont, M., Tulaczyk, S.M., Hubbard, B., Mankoff, K.D., Nicholls, K.W., Stewart, C.L., 2022. Rapid basal melting of the Greenland Ice Sheet from surface meltwater drainage. Proc. Natl. Acad. Sci. USA 119 (10). https://doi.org/10.1073/pnas.2116036119 e2116036119.
Ziegler, P.A., 1990. Geological Atals of Western and Central Europe. Geological Society, London.
Zoet, L.K., Iverson, N., 2020. A slip law for glaciers on deformable beds. Science 368 (6486), 76–78. https://doi.org/10.1126/science.aaz1183.
Zoet, L.K., Muto, A., Rawling, J.E., Attig, J.W., 2019. The effects of tunnel channel formation on the Green Bay Lobe. Geomorphology 324, 36–47. https://doi.org/10.1016/j.geomorph.2018.09.021. Wisconsin, USA.
Zwally, H.J., Abdalati, W., Herring, T., Larson, K., Saba, J., Steffen, K., 2002. Surface melt-induced acceleration of Greenland ice-sheet flow. Science 297 (5579), 218–222. https://doi.org/10.1126/science.1072708.
Zweck, C., Huybrechts, P., 2005. Modeling of the northern hemisphere ice sheets during the last glacial cycle and glaciological sensitivity. J. Geophys. Res. Atmos. 110. https://doi.org/10.1029/2004JD005489. D7.